Molecular Therapy
Original Article

Circular RNA circPDE4D Protects against Osteoarthritis by Binding to miR-103a-3p and Regulating FGF18

Yizheng Wu,[1,2,8] Zhenghua Hong,[1,2,3,8] Wenbin Xu,[1,2,8] Junxin Chen,[1,2] Qingxin Wang,[1,2,4] Jiaxin Chen,[5] Weiyu Ni,[1,2] Zixuan Mei,[1,2] Ziang Xie,[1,2] Yan Ma,[1,2] Jiying Wang,[1,2] Jianhong Lu,[6] Chao Chen,[7] Shunwu Fan,[1,2] and Shuying Shen[1,2]

[1]Department of Orthopaedic Surgery, Sir Run Run Shaw Hospital, Zhejiang University School of Medicine, Zhejiang, China; [2]Key Laboratory of Musculoskeletal System Degeneration and Regeneration Translational Research of Zhejiang Province, Zhejiang, China; [3]Department of Orthopaedic Surgery, Taizhou Hospital of Zhejiang Province, Zhejiang University School of Medicine, Zhejiang, China; [4]Department of Orthopaedic Surgery, China Coast Guard Hospital of the People's Armed Police Force, Zhejiang, China; [5]Department of Colorectal Surgery, Sir Run Run Shaw Hospital, Zhejiang University School of Medicine, Zhejiang, China; [6]Department of Clinical Laboratory, China Coast Guard Hospital of the People's Armed Police Force, Zhejiang, China; [7]Department of Orthopaedic Surgery, School of Traditional Chinese Medicine, Southern Medical University, Guangdong, China

Osteoarthritis (OA) is a common, age-related, and painful disease characterized by cartilage destruction, osteophyte formation, and synovial hyperplasia. This study revealed that circPDE4D, a circular RNA derived from human linear PDE4D, plays a critical role in maintaining the extracellular cellular matrix (ECM) during OA progression. circPDE4D was significantly downregulated in OA cartilage tissues and during stimulation with inflammatory cytokines. The knockdown of circPDE4D predominantly contributed to Aggrecan loss and the upregulation of matrix catabolic enzymes, including MMP3, MMP13, ADAMTS4, and ADAMTS5, but not proliferation or apoptosis. In a murine model of destabilization of the medial meniscus (DMM), the intraarticular injection of circPDE4D alleviated DMM-induced cartilage impairments. Mechanistically, we found that circPDE4D exerted its effect by acting as a sponge for miR-103a-3p and thereby regulated FGF18 expression, which is a direct target of miR-103a-3p. In conclusion, our findings highlight a novel protective role of circPDE4D in OA pathogenesis and indicate that the targeting of the circPDE4D-miR-103a-3p-FGF18 axis might provide a potential and promising approach for OA therapy.

INTRODUCTION

Osteoarthritis (OA) is an age-related disease that threatens the health of elderly people throughout the world, particularly individuals over 65 years of age.[1,2] OA is the leading cause of physical disability and thus imposes an enormous economic burden on society worldwide. The typical pathological changes in OA include cartilage destruction, osteophyte formation, and synovial hyperplasia. The most central and critical features in degenerated cartilage are the upregulation of matrix-degrading enzymes, including those belonging to the metalloproteinase (MMP) family and A disintegrin and metalloproteinase with thrombospondin motifs (ADAMTS) family, and loss of the extracellular matrix (ECM), which is mainly composed of glycosaminoglycan (GAG) and collagens.[3,4] Patients with OA usually exhibit various clinical manifestations, such as joint stiffness, local pain, and joint tenderness.[5] As a result, many different clinical management strategies focusing on the improvement of clinical symptoms have been developed and applied in clinical practice. However, no effective therapeutic interventions, with the exception of surgery, exert satisfying and curative effects on the progression of the disease.[6]

Circular RNA (circRNA) is a type of endogenous noncoding RNA that does not exhibit polarity or a polyadenylated tail in its structure[7] and is produced in a noncanonical manner called backsplicing in eukaryotes. The circRNA biogenesis process involves the formation of closed covalent loops with a specific junction site between the 3′ and 5′ splice sites of certain mRNAs through either base pairing between flanking intronic complementary sequences on both sides, such as *Alu elements*,[8,9] or dimerization of RNA-binding proteins (RBPs), such as protein quaking encoded by *QKI*.[10] In general, circRNAs have a relatively lower abundance compared with their linear counterparts. However, in certain cell types and tissues or under specific pathological conditions, some circRNAs are expressed at a higher level and can accumulate despite the relatively lower

Received 13 November 2019; accepted 1 September 2020;
https://doi.org/10.1016/j.ymthe.2020.09.002.

[8]These authors contributed equally to this work.

Correspondence: Shuying Shen, Department of Orthopaedic Surgery, Sir Run Run Shaw Hospital, Zhejiang University School of Medicine, Zhejiang, China.
E-mail: 11207057@zju.edu.cn
Correspondence: Shunwu Fan, Department of Orthopaedic Surgery, Sir Run Run Shaw Hospital, Zhejiang University School of Medicine, Zhejiang, China.
E-mail: 0099203@zju.edu.cn

efficiency of backsplicing compared with linear splicing.[11,12] Multiple functions of circRNAs have been identified. Several studies have revealed that circRNAs can function as miRNA sponges,[13–15] and among these circRNAs, CDR1as, which is also known as ciRS-7 and possesses approximately 74 canonical binding sites for miR-7, is one of the most characterized circRNAs in the neuroscience field.[16] In addition, circRNAs have also been found to act as "protein decoys,"[17] "protein function enhancers,"[18] "protein scaffolds,"[19,20] or "templates for translation."[21,22] Our previous study revealed that circSERPINE2 plays a critical role in OA pathogenesis by interacting with miR-1271 and its target gene, the ETS transcription factor ERG (ERG).[14] However, whether other circRNAs can regulate the initiation or progression of OA is not well understood, and their underlying mechanisms have not been elucidated.

In our study, we identified the highly expressed circPDE4D in OA, which is derived from the phosphodiesterase 4D (PDE4D) gene, and further explored its molecular mechanism in both primary human chondrocytes and an animal model in detail.

RESULTS

circPDE4D Is Downregulated in OA and Is Predominantly Localized in the Cytoplasm

Our previous study identified differentially expressed circRNAs between normal human cartilage and OA cartilage tissues (Figures S1A and S1B).[14] Here, we focused on circPDE4D, which was found to exhibit a significant differential expression. To determine whether the expression level of circPDE4D was decreased in human OA articular cartilage, we first collected cartilage specimens from OA patients undergoing total knee replacement and from patients with knee joint fracture and no history of OA (Figure S1C; Table S1); the degeneration severity of each specimen was macroscopically classified according to the Modified Outerbridge Classification[23,24] and further verified by Safranin-O/Fast green staining and Alcian blue staining. A marked decrease in circPDE4D was detected in OA cartilage chondrocytes by fluorescence *in situ* hybridization (FISH) analysis using a specific circPDE4D probe, and this decrease was associated with the degrees of degeneration and destruction in the OA cartilage samples with higher OA stages (Figure 1A). However, although the relative mRNA expression of circPDE4D obtained by qRT-PCR was negatively correlated with OA severity (Figure 1B), the linear form of PDE4D failed to show significant differences among cartilage specimens (Figure S1D), and Aggrecan and MMP3 served as positive indexes for specimen quality control in this analysis (Figures S1E and S1F). Because inflammatory activity is involved in OA pathogenesis and plays a critical role in OA progression,[25–27] we subsequently determined whether inflammatory stimuli could exert a certain influence on circPDE4D in primary human chondrocytes (HCs). As expected, tumor necrosis factor alpha (TNF-α) reduced circPDE4D expression in a dose-dependent manner (Figure S1G). In comparison, inflammatory stimulation did not induce a significant change in linear PDE4D expression (Figure S1H). The comparison of circPDE4D sequences acquired from circBase with the PDE4D mRNA sequences revealed that circPDE4D was looped and comprised exons 2–5 of its parental gene, and its head-to-tail splicing was further confirmed by Sanger sequencing (Figure 1C). In addition, convergent primers and specific divergent primers were designed to amplify PDE4D mRNA and circPDE4D. cDNA and gDNA (genomic DNA) were extracted from HCs and subsequently subjected to nucleic acid electrophoresis detection. Notably, circPDE4D could be amplified by the divergent primers from cDNA but not from gDNA, whereas PDE4D mRNA was detected in both the cDNA and gDNA samples (Figure 1D). Due to the previously reported high stability of circRNA,[7,16,28] we performed several experiments, including Northern blotting and qRT-PCR, to test whether circPDE4D exhibits high stability. As expected, even after treatment with RNase R, the band of interest (353 bp) with little degradation was detected using a DIG-labeled circPDE4D probe targeting the junction region (Figure 1E). Although circPDE4D was almost insensitive to RNase R, the linear PDE4D mRNA levels decreased sharply by more than 70% (Figure 1F). Additionally, actinomycin D, an inhibitor of transcription, was further applied to investigate the expression of circPDE4D under transcription-blocking conditions, and the results revealed that the half-life period of circPDE4D was significantly longer than that of its linear form (Figure 1G). Moreover, RNA FISH analysis and qRT-PCR demonstrated that circPDE4D was mainly localized in the cytoplasm (Figures 1H and 1I). These results demonstrate the critical characteristics of circPDE4D and indicate that circPDE4D, but not linear PDE4D transcripts, might have clinical significance for OA.

The Silencing of circPDE4D Induces Matrix Degradation in Chondrocytes

To investigate whether circPDE4D is involved in the regulation of OA, we generated three circPDE4D small hairpin RNAs (shRNAs) that could stably and specifically knock down circPDE4D in HCs and SW1353 cells. Because circPDE4D and linear PDE4D share a partial sequence, we also tested the effects of sh-circPDE4D on linear PDE4D mRNA (Figure 2A; Figure S2A). As shown in Figure 2B, glycosaminoglycan (GAG) was sharply reduced in sh-circPDE4D-treated chondrocytes. We also found that circPDE4D deficiency predominantly downregulated Aggrecan expression, whereas the matrix catabolic enzymes MMP3, MMP13, ADAMTS4, and ADAMTS5 were significantly upregulated at the mRNA level in both HCs and SW1353 cells (Figures 2C and 2D; Figures S2B and S2C), which was consistent with the results at protein level (Figure 2E; Figure S2D). Intriguingly, only a small difference in SOX9 and Col2a1 expression, if any, was detected in circPDE4D-deficient HCs and SW1353 cells, which indicated that circPDE4D was mainly involved in GAG but not collagen metabolism. In addition, we also constructed linear PDE4D-deficient HCs using two independent sh-PDE4Ds to determine the role of linear PDE4D in OA pathogenesis (Figure S3A), and we did not find any meaningful positive phenotypes (Figures S3B–S3E). During OA development, the cartilage microenvironment undergoes enormous changes compared with

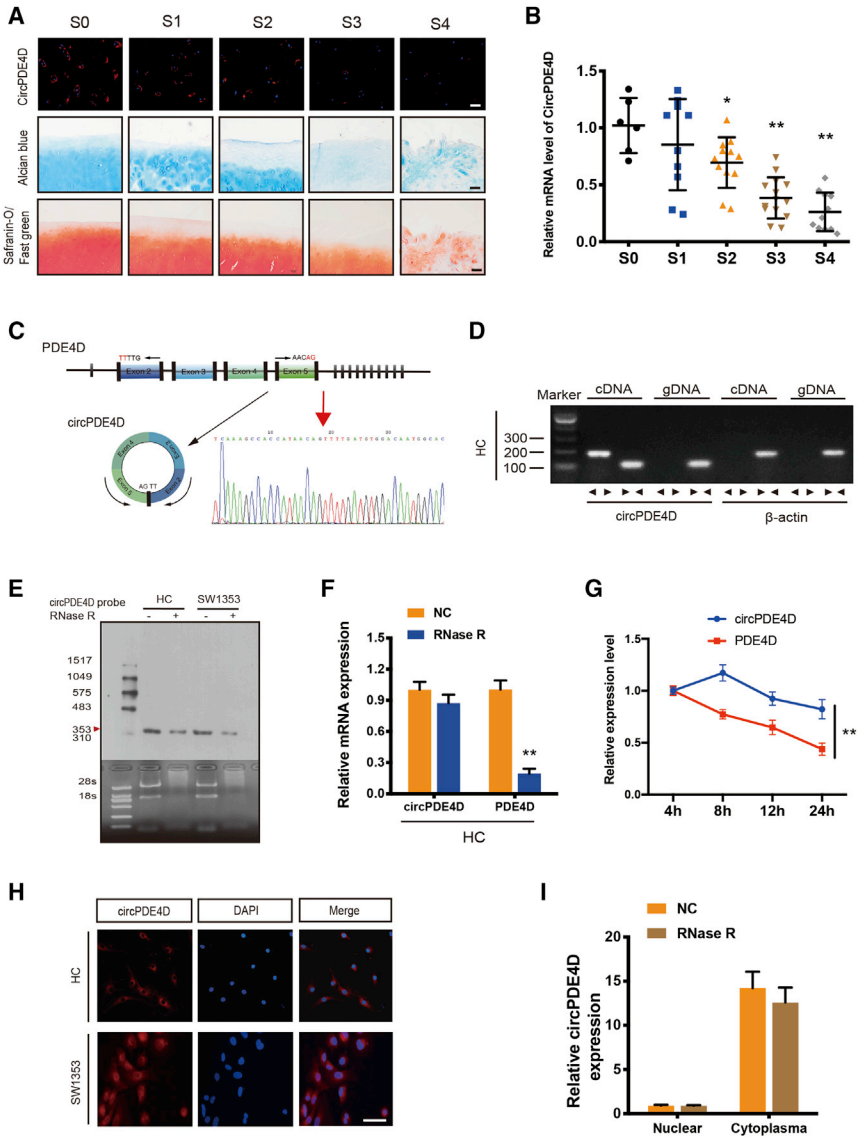

Figure 1. circPDE4D Validation and Expression in OA Cartilage Tissue and Chondrocytes

(A) Representative images of RNA fluorescence *in situ* hybridization (FISH), Safranin-O/Fast green staining and Alcian blue staining in human cartilage tissues from stage 0 (S0) to stage 4 (S4). Scale bar, 50 μm. (B) The expression of circPDE4D in human cartilage specimens from stage 0 (S0) to stage 4 (S4) (n = 53) was evaluated by qRT-PCR. (C) Schematic illustration demonstrating the circularization of PDE4D exon 2–5 to form circPDE4D (black arrow). The presence of circPDE4D was validated by RT-PCR followed by Sanger sequencing. The red arrow represents "head-to-tail" circPDE4D splicing sites. (D) The presence of circPDE4D in human HCs was validated by RT-PCR. Divergent primers amplified circPDE4D from cDNA but not from genomic DNA; β-actin served as the negative control. (E) Northern blots for detecting circPDE4D in HCs and SW1353 cells treated with or without RNase R. The upper panels show the probed blots of circPDE4D, and the red triangle represents the circPDE4D band size (353 bp). The lower panels show the gel electrophoresis results obtained for RNA with or without RNase R digestion. (F) The expression of circPDE4D and linear PDE4D mRNA in HCs treated with or without RNase R was detected by qRT-PCR. The relative levels of circPDE4D and PDE4D mRNA were normalized to the value obtained with the mock treatment. (G) The levels of circPDE4D and PDE4D in HCs treated with actinomycin D at the indicated time points were detected by qRT-PCR. (H) FISH showed that circPDE4D was predominantly localized in the cytoplasm. The circPDE4D probes were labeled with CY3, and nuclei were stained with DAPI. Scale bar, 20 μm. (I) circPDE4D was detected in different cell fractions. Nuclear and cytoplasmic RNA was extracted, and junction primers were used for circPDE4D detection. U6 was used as an internal control for nuclear RNA, and β-actin was used as an internal control for cytoplasmic RNA. The data were obtained from three independent experiments with three independent donors (presented as the means ± SDs; F, G, and I) or were representative of three independent experiments with similar results (A, B, D, E, and H). *$p < 0.05$ and **$p < 0.01$ versus the control or indicated group. The data were analyzed by one-way ANOVA followed by the Bonferroni test (B) and two-tailed t tests (F, G, and I).

those observed under healthy conditions, and inflammatory reactions,[26,29] metabolic stress,[27,30,31] and oxidative stress[32,33] are the most critical of these changes. Therefore, we treated HCs stably expressing sh-circPDE4D or control HCs with various stimuli. Surprisingly, treatment with inflammatory cytokines, including interleukin-1β (IL-1β), IL-6, and TNF-α, contributed to a markedly more severe OA phenotype compared with the matched control, as evaluated by Aggrecan expression (Figure 2F). We further explored whether circPDE4D could exert other effects (apoptosis or cell cycle) on the fate of chondrocyte (Figures S4A–S4C) but obtained no positive results. Therefore, we speculated that circPDE4D, but not linear PDE4D or might play a pivotal role in maintaining the chondrocyte extracellular matrix and alleviate inflammatory reactions in OA pathogenesis.

Blocking Endogenous circPDE4D Circularization Triggers ECM Degradation

In order to have a deeper understanding on the role of circPDE4D, we next investigated how circPDE4D was generated. Previous studies have reported several splicing factors contribute to regulating the circRNA formation by binding to the flanking introns during the alternative splicing,[7] among which QKI, DHX9, and ADAR1 are three most well-known regulators. However, we did not find the Alu elements in the flanking introns closing to circPDE4D (around 2,000 bp upstream and 5,000 bp downstream), which is necessary for the binding of DHX9[34] and ADAR1.[35] In comparison, abundant QKI response elements (QREs)[10,36] were found in both upstream and downstream flanking introns closing to circPDE4D (Figure S5A). RNA immunoprecipitation (RIP) analysis further

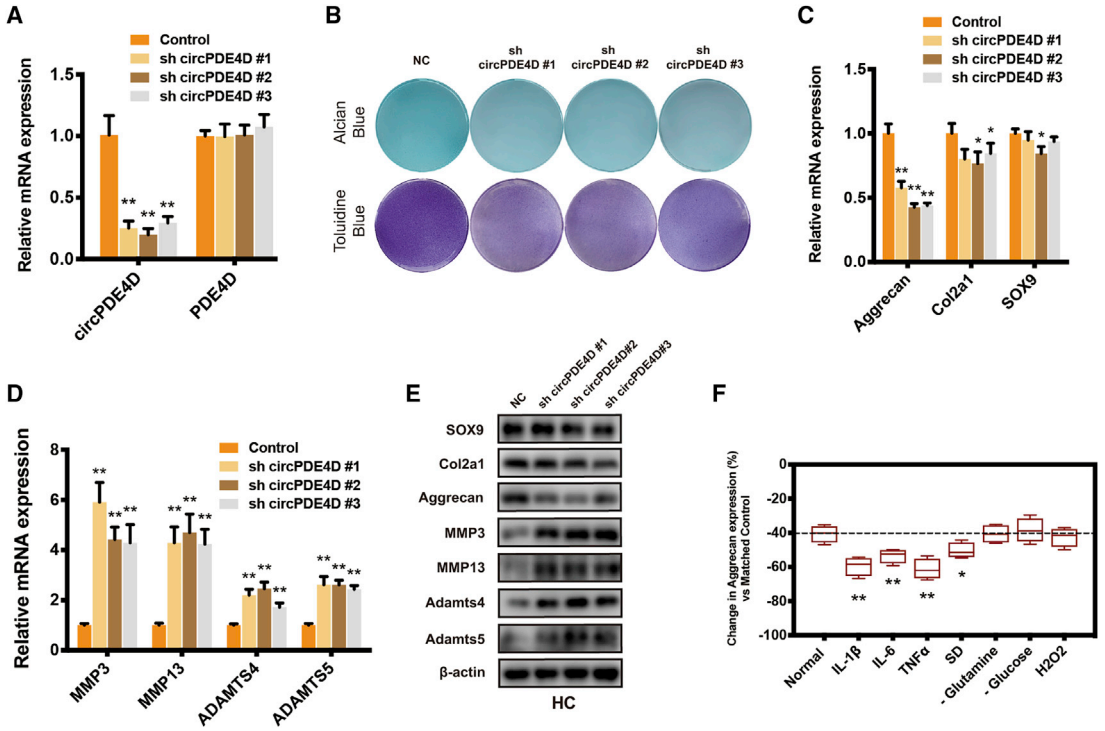

Figure 2. circPDE4D Knockdown Induced Matrix Degradation in Chondrocytes

(A) HCs were stably transfected with three different circPDE4D shRNAs or the negative control. The expression of circPDE4D and linear PDE4D was evaluated by qRT-PCR. (B) The cells were stably transfected with sh-circPDE4D #1, #2, or #3 or the negative control. Representative images of Alcian blue (SW1353) and toluidine blue staining (HCs) were shown. (C) The mRNA levels of matrix components Aggrecan, Col2a1, and SOX9 in HCs transfected with sh-circPDE4D #1, #2, #3 or negative control were evaluated by qRT-PCR. (D) The mRNA levels of catabolic enzymes MMP3, MMP13, ADAMTS4, and ADAMTS5 in HCs transfected with sh-circPDE4D #1, #2, #3 or negative control were evaluated by qRT-PCR. (E) The protein expression of Aggrecan, Col2a1, SOX9, MMP3, MMP13, ADAMTS4, and ADAMTS5 in sh-circPDE4D-treated HCs and control chondrocytes was determined by western blotting. (F) sh-circPDE4D-treated or vector control-treated HCs were stimulated with various inflammatory factors (IL-1β, IL-6, and TNF-α) or cultured under certain metabolic stress conditions (serum deprivation, glutamine deprivation, glucose deprivation, or oxidative stress). The histogram demonstrates the relative changes in Aggrecan expression compared with the matched control. The data were obtained from three independent experiments with three independent donors (presented as the means ± SDs; A, C, D, and F) or were representative of three independent experiments with similar results (B and E). *$p < 0.05$ and **$p < 0.01$ versus the control or indicated group. The data were analyzed using two-tailed t tests (A, C, D, and F).

confirmed the binding between QKI and flanking introns, but not circRNA or its remote introns (Figure S5B). circPDE4D, but not linear PDE4D or pre-PDE4D was significantly downregulated after QKI knockdown in both HCs and SW1353 cells, suggesting that circPDE4D could be regulated by QKI (Figures S5C–S5D). We then investigated whether deleting the circularization signal of circPDE4D could affect the ECM phenotypes in chondrocytes. Two guide RNAs targeting the both sides of upstream flanking sequences containing all the QREs were designed and simultaneously transfected into the SW1353 cells, with monoclonal cell further selected and cultured. Sanger sequencing confirmed the deletion by CRISPR-Cas9 (Figure S5E). qRT-PCR demonstrated that circPDE4D expression was predominantly downregulated after QREs deletion, suggesting that the endogenous circularization signal of circPDE4D was generally blocked (Figure S5F). Alcian blue and Toluidine blue staining showed that CRISPR-Cas9-edited SW1353 cells have much lower GAG content, which could partly be rescued by circPDE4D overexpression (Figure S5G). Additionally, the protein level of Aggrecan was significantly downregulated and the matrix catabolic enzymes were upregulated, which were alleviated by circPDE4D (Figure S5H). These results indicate that blocking endogenous circularization signal of circPDE4D leads to a lower circPDE4D abundance and the degradation of ECM.

circPDE4D Functions as a Sponge for miRNAs

circRNAs have previously been reported to play a major role in the RNA regulatory network by working as miRNA sponges to abrogate the function of miRNAs.[13–15] Given that circPDE4D is highly stable and predominantly localized in the cytoplasm, we subsequently investigated whether circPDE4D regulates OA pathogenesis via a miR sponge mechanism. The overlapping results from two online databases (RNAhybrid and TargetScan) and the upregulated miRNA sequences in OA cartilage tissues identified in our previously reported study yielded 15 miRNA candidates (Figure 3A; Figure S6A).[14] We then performed a pull-down assay using a biotinylated-circPDE4D probe and selected three possible miRNAs (miR-103a-3p, miR-107,

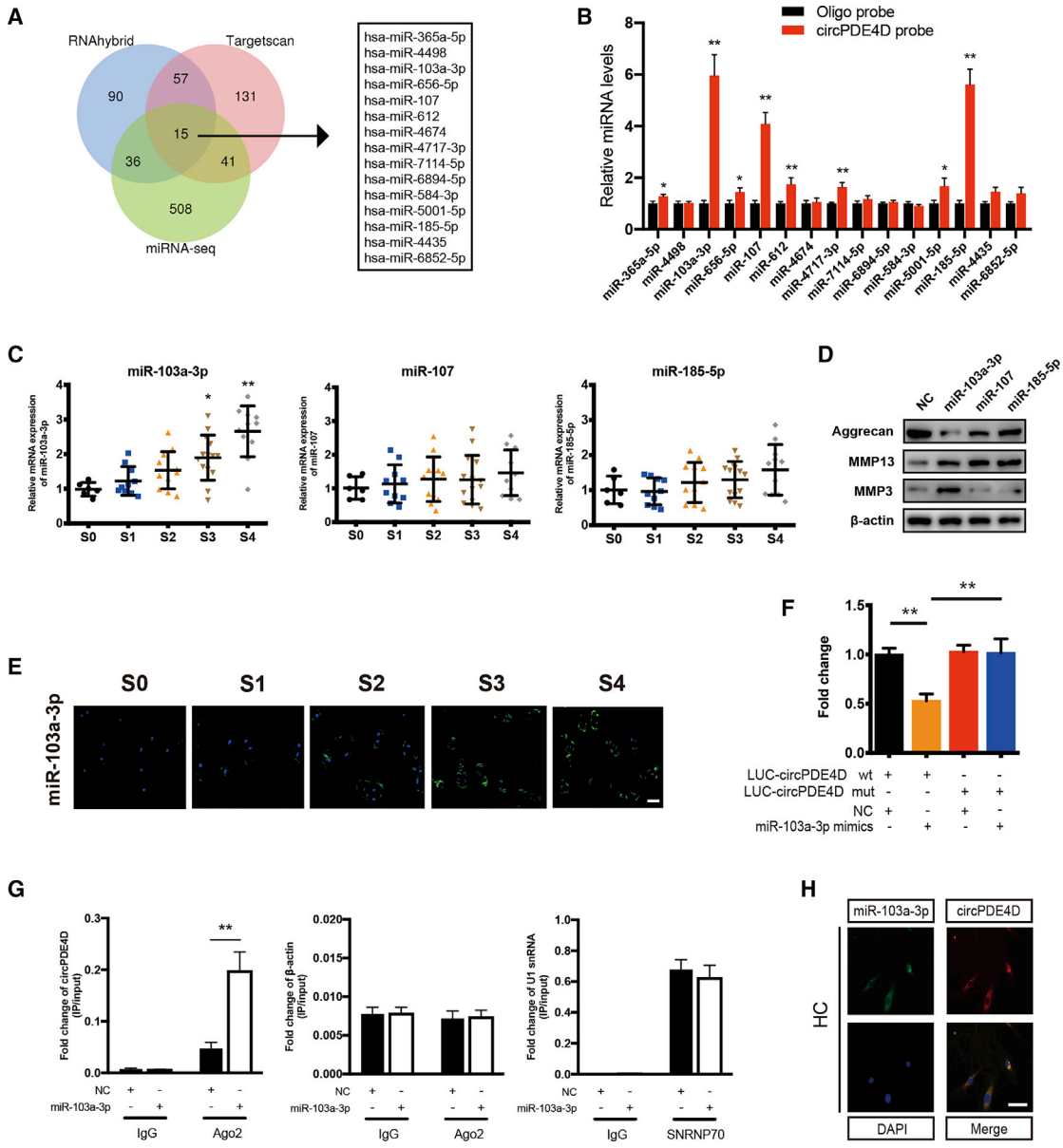

Figure 3. circPDE4D Serves as a Sponge for miR-103a-3p in Human Chondrocytes

(A) Schematic illustration showing the overlap of the potential target miRNAs of circPDE4D predicted using the RNAhybrid and TargetScan databases and the miRNA sequences. (B) The relative levels of 15 miRNA candidates in HC lysates after pull-down assay were examined by qRT-PCR. Multiple miRNAs were pulled down by circPDE4D. (C) The expression of miR-103a-3p, miR-107, and miR-185-5p in human cartilage tissues (stage 0 to stage 4) was evaluated by qRT-PCR (n = 53). (D) HCs were transfected with miR-103a-3p, miR-107, miR-185a-5p, or negative control and then used for detection of Aggrecan, MMP3, and MMP13 proteins. (E) Representative images of FISH demonstrating the relative expression of miR-103a-3p in human cartilage tissues (stages 0–4). The corresponding Safranin-O/Fast green staining and Alcian blue staining are shown in Figure 1A. Scale bar, 50 μm. (F) HEK293T cells were transfected with miR-103a-3p (or NC) and circPDE4D reporter (or circPDE4D mut reporter) and then used for luciferase activity detection. (G) The circPDE4D levels in SW1353 cells transfected with NC or miR-103a-3p were detected by Ago2 RNA immunoprecipitation assay (RIP assay). IgG was used as a control, and β-actin was used as a negative control. SNRNP70 RIP for U1 snRNA was used as a positive control. (H) FISH images showing the colocalization of circPDE4D and miR-103a-3p in HCs. miR-103a-3p probes were labeled with Alexa Fluor 488. Locked nucleic acid circPDE4D probes were labeled with CY3, and nuclei were stained with DAPI. Scale bar, 20 μm. The data were obtained from three independent replicates (presented as the means ± SDs; B and G) or were obtained from three independent replicates (F) or were representative of three independent experiments with similar results (C, E, and H). *$p < 0.05$ and **$p < 0.01$ versus the control or indicated group. The data were analyzed by one-way ANOVA followed by the Bonferroni test (C) and two-tailed t tests (B, F, and G).

and miR-185-3p) that showed significantly enhanced fold-changes in circPDE4D capture in HCs (Figure 3B). Notably, miR-103a-3p increased with increases in the cartilage stages, whereas no significant difference in miR-107 and miR-185-3p was found among cartilage specimens by qRT-PCR detection (Figure 3C). We also found that the expression of pre-miR-103a-3p did not change with changes in the OA stage, which indicates that the upregulation of miR-103a-3p in clinical samples is mainly due to the role of circPDE4D as a miRNA sponge rather than its effects on transcription or miRNA processing (Figure S6B). To assess the function of these three miRNAs, we separately constructed corresponding mimics, transfected them into HCs, and evaluated the resulting changes in the Aggrecan, MMP13, and MMP3 protein levels by western blotting (Figure 3D). All selected miRNAs significantly upregulated MMP13, but only miR-103a-3p resulted in both decreased Aggrecan levels and increased MMP3 expression. Therefore, miR-103a-3p was selected for subsequent studies. Accordingly, a FISH analysis using a specific probe revealed a predominantly enhanced fluorescence intensity for miR-103a-3p in cartilages with higher stages compared with those with lower stages (Figure 3E). We subsequently investigated the binding between circPDE4D and miR-103a-3p by generating a circPDE4D luciferase plasmid (WT) and a mutant plasmid (Mut) and separately cotransfecting them into HEK293T cells with miR-103a-3p. The luciferase assay showed a markedly stronger luciferase intensity in the circPDE4D mutant group compared with the WT group, which indicated that miR-103a-3p can directly bind to circPDE4D (Figure 3F; Figure S6C). An Ago2-RIP analysis using SW1353 cells was conducted to confirm this finding, and the results revealed that circPDE4D could be preferentially pulled down after the overexpression of miR-103a-3p (Figure 3G). Moreover, the colocalization (cytoplasm) of miR-103a-3p and circPDE4D was revealed by FISH (Figure 3H; Figure S6D). To further investigate the response of circPDE4D and miR-103a-3p to inflammatory cytokines, we performed a Pearson correlation analysis after TNF-α stimulation at different time points and found that circPDE4D exhibited a negative correlation with miR-103a-3p under inflammatory conditions (Figures S6E–S6G). These data suggested that miR-103a-3p can directly interact with circPDE4D.

miR-103a-3p Triggers Chondrocyte Matrix Degradation

Because miR-103a-3p exhibited predominant differential expression between OA and normal cartilage tissues and could be directly regulated by circPDE4D, we subsequently explored whether miR-103a-3p plays a role in OA development. HCs were stably transfected with miR-103a-3p or miR-103a-3p sponges (Figure 4A) and then subjected to Alcian blue and toluidine blue staining (Figure 4B). As expected, the GAG content was significantly decreased by miR-103a-3p and moderately, if at all, increased by the miR-103a-3p sponge. Additionally, miR-103a-3p sharply downregulated Aggrecan and upregulated the mRNA and protein expression of MMP3, MMP13, ADAMTS4, and ADAMTS5 in HCs. Conversely, miR-103a-3p-deficient HCs and SW1353 cells exhibited markedly higher Aggrecan expression and inhibition of matrix catabolic enzymes (Figures 4C–4E). We also found that the mRNA expression of both circPDE4D and PDE4D was not affected by miR-103a-3p overexpression (Figure S6H). A previous study found that miR-103a-3p serves as a tumor suppressor by suppressing proliferation and promoting apoptosis in glioma stem cells.[37] Lu et al.[38] reported that circTCF25-regulated miR-103a-3p could inhibit both proliferation and migration *in vitro* and *in vivo* in bladder cancer. Therefore, we also investigated whether miR-103a-3p influences the pathogenesis of OA in other aspects. However, flow cytometry and western blotting analyses suggested that miR-103a-3p failed to contribute to apoptosis and cell cycle progression in chondrocytes (Figure S7A–S7C). Overall, these results suggested that matrix degeneration, but not apoptosis or the cell cycle, could be induced by miR-103a-3p.

The Silencing of miR-103a-3p Reverses sh-circPDE4D-Induced Matrix Degeneration in Chondrocytes

To explore whether circPDE4D enhances catabolic enzymes and reduces Aggrecan expression by interacting with miR-103a-3p, we cotransfected sh-circPDE4D and a miR-103a-3p sponge into HCs and SW1353 cells and performed FISH to determine the resulting changes in the expression of circPDE4D and miR-103a-3p (Figure 5A). A qRT-PCR analysis also confirmed the mRNA levels of circPDE4D and miR-103a-3p (Figures S8A–S8D). Alcian blue and toluidine blue staining demonstrated that the circPDE4D knockdown-induced loss of GAG could be reversed by the miR-103a-3p sponge (Figure 5B). Subsequently, qRT-PCR and western blotting analyses were performed, and the results suggested that the miR-103a-3p sponge partly reversed the OA phenotype in HCs and SW1353 cells, as demonstrated by the substantial decreases in the mRNA and protein expression levels of MMP3, MMP13, ADAMTS4, and ADAMTS5 and the increased expression of Aggrecan in circPDE4D-deficient HCs expressing the miR-103a-3p sponge (Figures 5C–5E; Figures S8E–S8G). Because circPDE4D and its mouse homolog mmu-circPDE4D share very high conservation and homology with 93.2% sequence similarity (Figure S8H), 12-week-old mice undergoing destabilization of the medial meniscus (DMM) or sham surgery were administered an articular injection of si-NC, si-mmu-circPDE4D, or both si-mmu-circPDE4D and miR-103a-3p antagomir to evaluate the "circPDE4D-miR-103a-3p" axis *in vivo*, and the expression of this axis was confirmed by FISH (Figure S8I). Notably, mmu-circPDE4D knockdown in mouse cartilage could trigger articular degeneration and surface abrasion even without DMM surgery. These articular impairments and the biochemical changes in Aggrecan and MMP3 could be partly reversed by the overexpression of miR-103a-3p antagomir with or without DMM surgery (Figures 5F–5I). Based on these results, circPDE4D acts as a functional sponge of miR-103a-3p to regulate the balance between catabolism and anabolism in chondrocytes *in vitro* and *in vivo*.

miR-103a-3p Directly Targets FGF18

To gain a more in-depth understanding of the effects of circPDE4D and miR-103a-3p, we screened the transcriptome by RNA sequencing (RNA-seq) by focusing on the differentially expressed genes between HCs with stable circPDE4D knockdown and control HCs, and the resulting heatmap, volcano plot, and scatter diagram are shown in

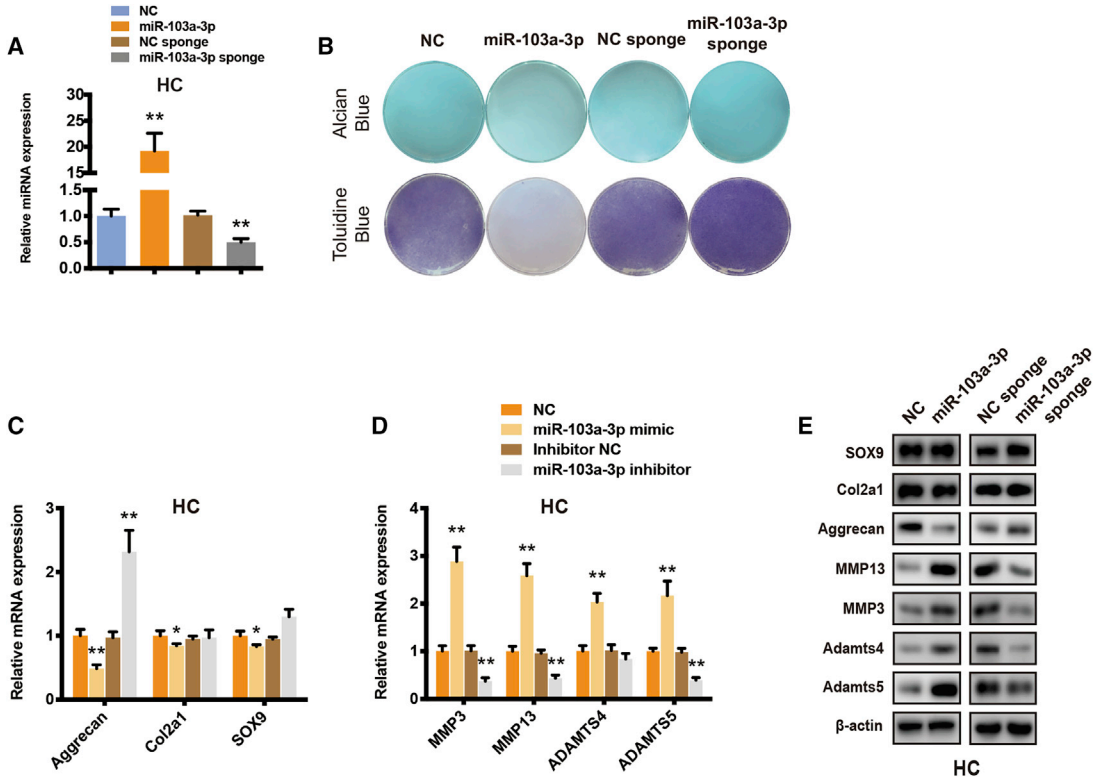

Figure 4. Cartilage Matrix Degradation Can Be Triggered by miR-103a-3p in Chondrocytes

(A) Human chondrocytes were stably transfected with miR-103a-3p, miR-103a-3p sponge, or negative control. The expression of miR-103a-3p was measured by qRT-PCR and normalized to U6 expression. (B) Alcian blue (SW1353) and toluidine blue staining (HCs) in the corresponding treatments was measured. (C) The mRNA levels of Aggrecan, Col2a1 and SOX9 in stable HCs were detected by qRT-PCR. (D) The mRNA levels of MMP3, MMP13, ADAMTS4 and ADAMTS5 in stable HCs were evaluated by qRT-PCR. (E) The changes in the protein expression of Aggrecan, Col2a1, SOX9, MMP3, MMP13, ADAMTS4, and ADAMTS5 in HCs were evaluated by western blotting. The data were obtained from three independent experiments with three independent donors (presented as the means ± SDs; A, C, and D) or were representative of three independent experiments with similar results (B and E). *$p < 0.05$ and **$p < 0.01$ versus the control or indicated group. The data were analyzed by two-tailed t tests (A, C, and D).

Figures 6A–6C. Notably, the RNA-seq data revealed that major members of the MMP family, ADAMTS family, and IL family were significantly upregulated in circPDE4D-deficient HCs, whereas ACAN (Aggrecan) and major participants of the tissue inhibitor of metalloproteinase (TIMP) family were sharply reduced (Figure 6D). These data suggested that the knockdown of circPDE4D could trigger activated catabolism and an inflammatory cascade, and conversely attenuate anabolism, which is in accordance with our above-described data. We subsequently investigated the possible targets of miR-103a-3p and circPDE4D by overlapping the predicted results for miR-103a-3p obtained through a TargetScan analysis with the RNA-seq data. Four selected candidates (THY, DEPTOR, FGF18, and SNURF) were knocked down by specific siRNAs in HCs, and the resulting knockdown was evaluated by qRT-PCR (Figure S9A) and western blotting (Figure S9B). Among these four genes, FGF18 was the only gene that simultaneously enhanced anabolism and suppressed catabolism in HCs, and thus, FGF18 was selected for further study. As expected, circPDE4D-deficient HCs exhibited decreased FGF18 expression (Figure 6F), and FGF18 was significantly decreased in cartilage specimens with higher stages of OA (Figure 6G). Direct evidence of the binding between miR-103a-3p and FGF18 was obtained through luciferase assays using HEK293T cells cotransfected with FGF18 luciferase reporter (WT or Mut) and miR-103a-3p. The data showed that miR-103a-3p strongly decreased the luciferase activity in the cells transfected with FGF18 3′-UTR-WT but not in the cells transfected with the FGF18 3′-UTR-Mut (Figure 6H; Figure S9C). Notably, the complementary sequence between miR-103a-3p and FGF18 in different species was largely conserved, which suggested high evolutionary conservation across various species (Figure S9D). Moreover, both the mRNA and protein levels of FGF18, together with those of its previously reported downstream targets p-FGFR3 and p-ERK1/2[39–42] (Figure S9E), was downregulated by sh-circPDE4D and miR-103a-3p and conversely upregulated by the miR-103a-3p sponge in HCs (Figures 6I–6K). We subsequently transfected FGF18 expression plasmids into circPDE4D-deficient HCs and surprisingly observed that the expression of Aggrecan and the matrix catabolic enzymes MMP3, MMP13, ADAMTS4, and ADAMTS5 could be partly reversed by this transfection. In conclusion, these data indicated that FGF18 is a direct target of miR-103a-3p and plays a protective role against degeneration in chondrocytes.

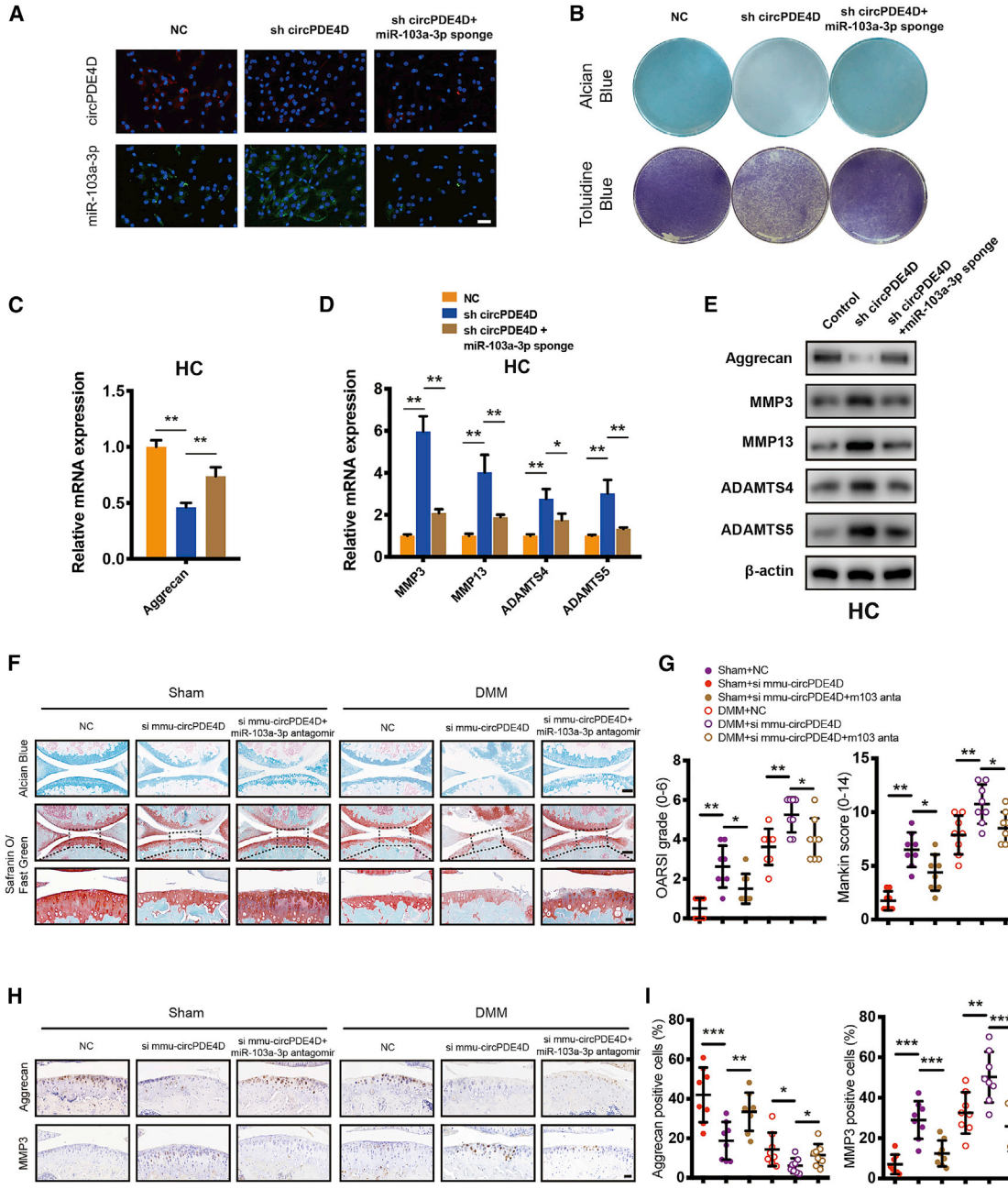

Figure 5. The Knockdown of miR-103a-3p Reverses sh-circPDE4D-Induced Cartilage Degradation

(A) HCs were stably transfected with sh-circPDE4D or with both sh-circPDE4D and miR-103a-3p sponge. FISH revealed the fluorescence intensity of circPDE4D (red) and miR-103a-3p (green). miR-103a-3p probes were labeled with Alexa Fluor 488, and circPDE4D probes were labeled with CY3. Scale bar, 50 μm. (B) Stably transfected cells were cultured and then subjected to Alcian blue (SW1353) and toluidine blue staining (HCs). (C) The mRNA expression of Aggrecan, in HCs was detected by qRT-PCR. (D) The mRNA expression of MMP3, MMP13, ADAMTS4, and ADAMTS5 in HCs was detected by qRT-PCR. (E) Western blotting demonstrated the expression of Aggrecan, MMP3, MMP13, ADAMTS4, and ADAMTS5 in stable HCs. (F) 12-week-old mice undergoing DMM or sham surgery were administered si-NC, si- mmu-circPDE4D, or both si-mmu-circPDE4D + miR-103a-3p antagomir via articular injection. Representative images of Safranin-O/Fast green and Alcian blue staining are shown. (n = 8 each group.) Scale bar, 100 and 20 μm. (G) The corresponding OARSI grades and Mankin score diagrams are shown. (H) Representative images of IHC for Aggrecan and MMP3 in mouse cartilage are shown. Scale bar, 20 μm. (I) Statistical diagrams of IHC for Aggrecan and MMP3. The data were obtained from three independent experiments with three independent donors (presented as the means ± SDs; C and D) or were representative of three independent experiments with similar results (A and B). *$p < 0.05$ and **$p < 0.01$ versus the control or indicated group. The data were analyzed by two-tailed t tests (C, D, G, and I).

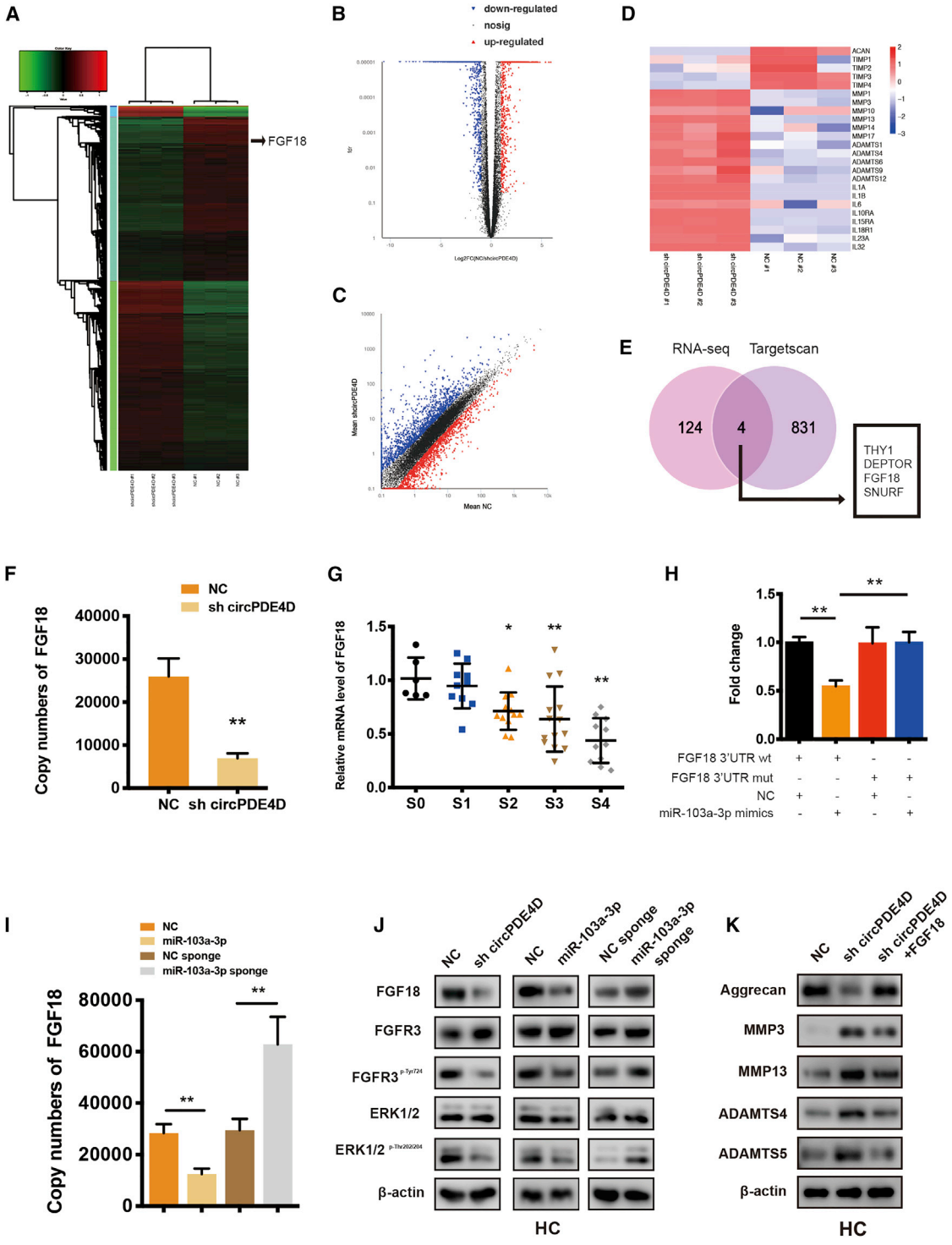

Figure 6. FGF18 Is the Direct Target of miR-103a-3p and Mediates the Function of miR-103a-3p and circPDE4D

(A) Clustered heatmap of differentially expressed mRNAs in HCs stably transfected with NC or sh-circPDE4D. (B) In the volcano plot, significantly upregulated genes are represented by red dots, whereas significantly downregulated genes are represented by blue dots. (C) The scatter diagram shows the differently expressed genes. (D) Representative genes involved in cartilage anabolism, catabolism, or inflammation identified from the RNA-seq data. (E) Schematic diagram exhibiting the overlap between the downregulated mRNAs identified from the RNA-seq data (Log_2(sh-circPDE4D/NC) < −2.5, $p < 0.01$) and target gene analyses of miR-103a-3p using the TargetScan

(legend continued on next page)

The Injection of circPDE4D Alleviates DMM-Induced OA in a Mouse Model

To investigate the functions of circPDE4D and miR-103a-3p *in vivo*, we intraarticularly administered adeno-associated virus (AAV) circPDE4D (WT or Mut; Figures S10A and 10B) to DMM-induced OA mice. 12 weeks after surgery, Safranin-O/Fast green and Alcian blue staining (Figure 7A) was performed to evaluate the degree of cartilage matrix degradation, and FISH (Figure S10C) and qRT-PCR analyses (Figure S10D) were performed to confirm the expression of circPDE4D after AAV injection. The degree of cartilage impairment in DMM-induced OA mice was improved by AAV-circPDE4D-WT injection but not by AAV-circPDE4D-Mut injection. A quantitative analysis indicated that the AAV-circPDE4D-injected mice demonstrated significantly lower Osteoarthritis Research Society International (OARSI) scores and Mankin scores, whereas the AAV-circPDE4D-Mut-injected mice had scores similar to those obtained for DMM mice (Figure 7B). As expected, miR-103a-3p was predominantly upregulated in DMM-induced impaired cartilage, and this upregulation could be reversed by circPDE4D but not circPDE4D-Mut. Moreover, circPDE4D, but not circPDE4D-Mut, reversed the loss of Aggrecan, the upregulation of matrix catabolic enzymes, and FGF18 expression, as evaluated by immunohistochemistry (IHC; Figures 7C and 7D), which was consistent with the qRT-PCR results obtained for mouse cartilage tissues (Figures S10E and 10F). Before euthanasia, the mice were subjected to the hot plate and rotarod tests (Figures 7E and 7F) to determine the existence of ethological changes. Interestingly, the mice administered the circPDE4D AAV injection after DMM surgery showed markedly improved performance in terms of pain assessment and endurance evaluation compared with the DMM-induced mice and the mice administered the circPDE4D-Mut AAV injection after DMM surgery. Taken together, these results revealed the positive effects of circPDE4D on suppressing ECM catabolism and promoting anabolism in OA pathogenesis and consequently alleviating OA progression *in vivo* (Figure 7G).

DISCUSSION

OA, which is characterized by cartilage destruction, osteophyte formation, and synovial hyperplasia, is an age-related or posttraumatic disease with very high morbidity in the elderly population and is mainly caused by cartilage matrix anabolism and catabolism imbalance. Studies aiming to understand OA pathogenesis and progression have mainly focused on the key factors regulating the cartilage extracellular matrix (ECM) or catabolic process.[43–45] Here, we demonstrated that circPDE4D expression is downregulated in OA cartilage specimens or during stimulation with inflammatory cytokines and found that circPDE4D plays a critical role in maintaining the GAG composition and simultaneously inhibiting matrix degeneration enzymes by sponging miR-103a-3p and regulating FGF18 expression.

Phosphodiesterase 4D (PDE4D) is a protein-coding gene, and the encoded protein possesses 3′,5′-cyclic-AMP phosphodiesterase activity and degrades the second messenger cAMP, which is a critical signaling transductor in many important pathways. Previous studies have revealed that PDE4D is involved in stroke pathogenesis, particularly in atherosclerosis-associated stroke, possibly by regulating vessel immunity and smooth muscle cell proliferation.[46,47] In addition, Mishra et al.[48] reported that PDE4D plays a critical role in acquired tamoxifen-resistant breast cancer through the inhibition of cAMP/ER stress/p38-JNK signaling and apoptosis. However, the role of circPDE4D, which was identified by circRNA sequences in our previous study, in any disease or any physiological process is not well understood.

We determined that circPDE4D, which was significantly downregulated in OA cartilage, originates from exons 2–5 of PDE4D and forms a ring structure by connecting the 3′ and 5′ splice sites. Even under RNase R treatment, circPDE4D still demonstrated very high stability and integrity, similarly to most circRNAs.[7,16,28] Therefore, we believe that circRNAs, including circPDE4D, can serve as stable markers for diagnosis or prognosis or even therapeutic targets for certain diseases. Moreover, the present study revealed that circPDE4D is highly conserved between humans and mice with 93.2% sequence homology and that the binding sequence between miR-103a-3p and FGF18 also shares very high conservation across various vertebrates. Because both circRNA and its linear mRNA form are generated from the same RNA precursor, the design of specific knockdown molecular tools that do not affect other transcripts is extraordinarily difficult. Fortunately, we successfully engineered specific short hairpin RNA that targets the junction spite of circPDE4D without affecting the expression of the linear PDE4D, and subsequent functional experiments suggested that circPDE4D protected chondrocytes against ECM degeneration in a PDE4D-independent manner. Interestingly, circPDE4D knockdown can exert synergistic effects with inflammation, and this synergism contributes to a markedly more severe ECM degradation phenotype. This finding could partly be explained

database. (F) mRNA expression of FGF18 in HCs stably transfected with sh-circPDE4D. (G) The expression of FGF18 in human cartilage tissues (stage 0 to stage 4) was determined by qRT-PCR. The corresponding Safranin-O/Fast green staining and Alcian blue staining are shown in Figure 1A (n = 53). (H) HEK293T cells were cotransfected with miR-103a-3p (or NC) and luciferase reporter constructs containing wild-type (WT) or mutated FGF18 3′-UTR. The relative luciferase activity is demonstrated in the histogram. (I) Effect of miR-103a-3p on the mRNA expression of FGF18. Chondrocytes were transfected with miR-103a-3p/miR-103a-3p sponge or the corresponding NC and then used for qRT-PCR analysis. (J) The protein expression of FGF18, FGFR3, FGFR3$^{p\text{-}Tyr724}$, ERK1/2, and ERK1/2$^{p\text{-}Thr202/204}$ in HCs was detected by western blotting. Cells were transfected with sh-circPDE4D, miR-103a-3p, miR-103a-3p sponge, or the corresponding NC. (K) HCs stably transfected with sh-circPDE4D (or NC) or cotransfected with sh-circPDE4D and FGF18 were subjected for the western blotting detection of Aggrecan, MMP3, MMP13, ADAMTS4, and ADAMTS5. The data were obtained from three independent experiments with three independent donors (presented as the means ± SDs; F and I), were obtained from three independent replicates (H) or were representative of three independent experiments with similar results (G, J, and K). *$p < 0.05$ and **$p < 0.01$ versus the control or indicated group. The data were analyzed by one-way ANOVA followed by the Bonferroni test (G) and two tailed t tests (F, H, and I).

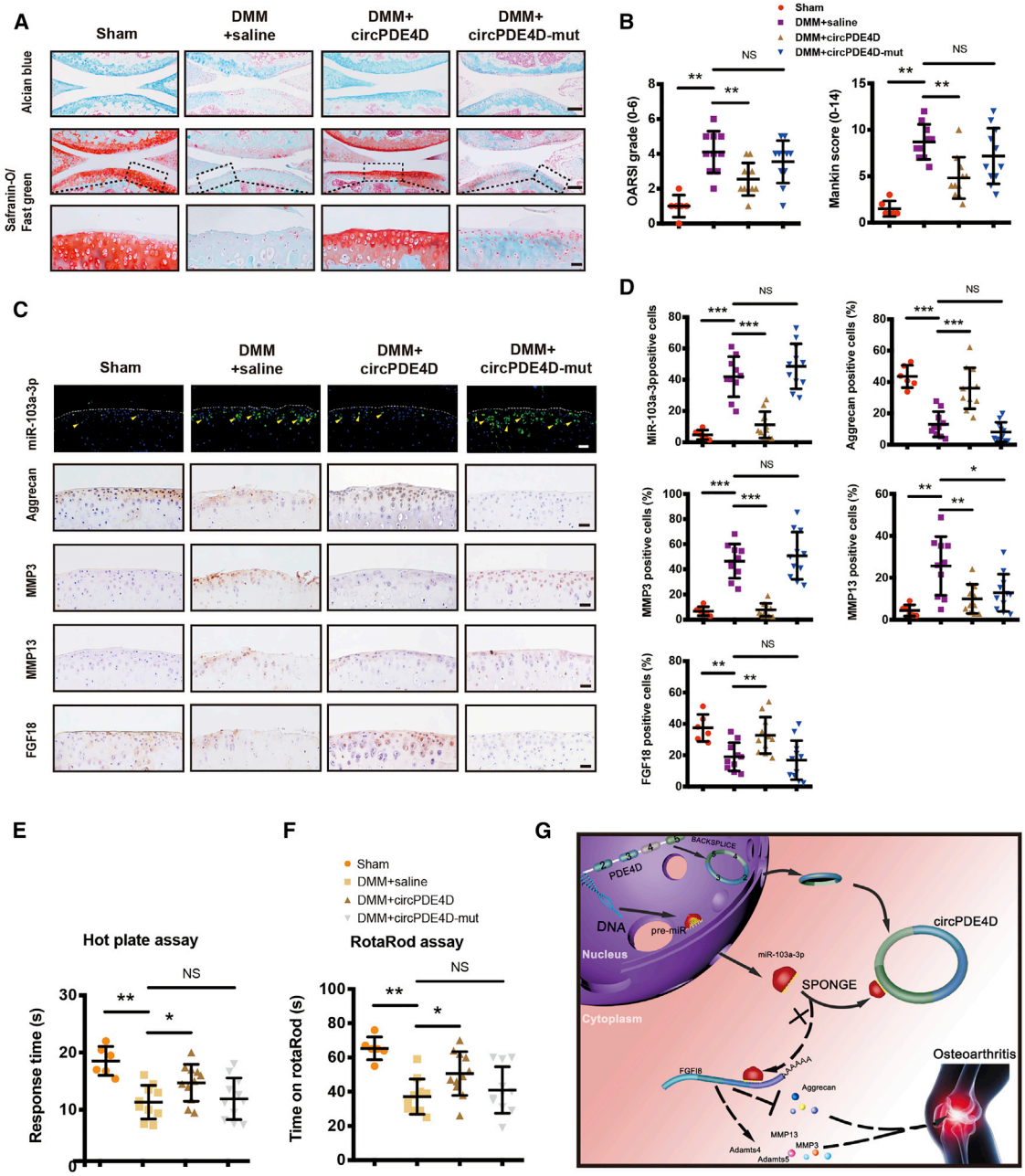

Figure 7. Articular Injection of circPDE4D Alleviates DMM-Induced OA in Mice

(A and B) Mice underwent sham surgery, DMM surgery with 0.9% saline intraarticular injection, DMM surgery with circPDE4D-WT AAV intraarticular injection, or DMM surgery with circPDE4D-Mut AAV injection. The corresponding Alcian blue and Safranin-O/Fast green staining (A) and the statistical OARSI grades and Mankin score diagrams (B) are shown. Scale bar, 100 and 20 μm (Sham, n = 6; DMM, n = 10; DMM+circPDE4D, n = 11; and DMM+circPDE4D-Mut, n = 11). The corresponding timeline is shown in Figure S7A. (C and D) Representative images (C) and statistical diagrams (D) of miR-103a-3p FISH and IHC of Aggrecan, MMP3, MMP13, and FGF18. Scale bar, 20 μm. (E and F) Response time on a hot plate at 55°C (E) and time on rotarods (F) obtained with the mice after sham or DMM surgery with (or without) circPDE4D-WT (or circPDE4D-Mut) AAV injection. (G) Schematic of the working hypothesis for circPDE4D. The data were obtained from three independent experiments (presented as the means ± SDs; B, D, E, and F) or were representative of three independent experiments with similar results (A and C). *$p < 0.05$ and **$p < 0.01$ versus the control or indicated group. The data were analyzed by two-tailed t tests (B, D, E, and F).

by the observation that cotreatment with inflammatory cytokines, such as TNF-α, and sh-circPDE4D led to markedly lower circPDE4D expression. Synergy is also observed in the culture of chondrocytes without sufficient nutrition or growth factors. These microenvironment alterations are extradentary similar to those observed during OA initiation and progression. Thus, local supplementation with exogenous circPDE4D using certain approaches is very likely to exert positive effects on OA prevention or therapeutic effects. Except for that, we identified the QKI-mediated endogenous circularization signaling in circPDE4D formation and constructed two guide RNAs targeting both side of flanking sequences containing QREs via CRISPR-Cas9. Similar ECM degradation phenotypes were obtained in endogenous CRISPR-Cas9-editing cells as using exogenous gene knocking down tools. Hwang et al.[49] reported that hypocellular cartilage with lacunar emptying could be observed in late-stage OA, which indicated that chondrocyte death is tightly associated with OA pathogenesis. Although a distinct and powerful regulatory effect of circPDE4D on ECM anabolism and catabolism has been revealed, we did not find any involvement of this circRNA in cell proliferation or apoptosis in this study.

FGF18 is a member of the fibroblast growth factor (FGF) family and plays a central role in skeletal growth and development.[50–52] Of interest, a recent genome-wide association study (GWAS) of osteoarthritis demonstrated that FGF18 has cartilage regeneration properties and exerts therapeutic effects on osteoarthritis in clinical practice.[53] FGF18 specifically activates FGFR3 in the growth plate and chondrocytes and participates in skeletal development and chondrogenesis.[39,50,52,54] Furthermore, FGF18 stimulates proliferation and ECM production in a healthy chondrocyte monolayer.[51,55] In addition, the injection of sprifermin (during clinical development of recombinant human FGF18) into the knee of patients with OA induces a dose-dependent increase in the cartilage volume and reduced cartilage loss.[56] Accumulating evidence suggests that the well-known competitive endogenous RNA (ceRNA) network, which reveals an intricate interplay among diverse RNA species, plays a critical role in various physiological processes and multiple diseases.[14,15,57,58] Based on this theory, coding and noncoding RNAs could establish a large regulatory RNA network via crosstalk with microRNA elements (MREs; lncRNA-miRNA-mRNA axis) across the transcriptome.[59] Here, FGF18 was identified as a direct target of miR-103a-3p and was found to be regulated by circPDE4D. Notably, we demonstrated that FGF18 expression or a miR-103a-3p sponge could partly restore the circPDE4D-induced loss of Aggrecan and upregulation of catabolic enzymes (MMP3, MMP13, ADAMTS4, and ADAMTS5), which indicated that circPDE4D works through miR-103a-3p and its downstream target FGF18 in OA pathophysiology.

In this study, a large number of gain-of-function, loss-of-function, and rescue experiments *in vivo* and *in vitro* together with a DMM mouse model administered an AAV intraarticular injection were performed to reveal a pivotal role for circPDE4D and its underlying mechanism. However, due to the high homology between human and murine circPDE4D, additional data are needed to evaluate FGF18 deficiency in genetically engineered mouse models of OA. In addition, because aberrant subchondral remodeling and synovitis are also the crucial causes of OA, future studies will comprehensively explore the involvement of circPDE4D in the subchondral bone region or synovium rather than only at the cartilage level.

In summary, we found that circPDE4D is significantly decreased in OA cartilage tissues and during stimulation with inflammatory cytokines. The circPDE4D-miR-103a-3p-FGF18 axis might serve as a novel and critical target in the treatment of OA. The administration of circPDE4D and FGF18 might alleviate catabolism in chondrocytes and protect the ECM from degradation.

MATERIALS AND METHODS

Human Cartilage and OA Mouse Model

Human cartilage specimens were collected according to protocols approved by the Ethics Committee of Sir Run Run Shaw Hospital (Zhejiang, China), and the experiments were performed in accordance with the approved guidelines. Written informed consent was obtained from all the subjects. Control cartilage tissues were obtained from patients with knee joint fracture and no history of OA (n = 6), whereas pathological cartilage tissues were acquired from patients with end-stage symptomatic knee OA at the time of total knee replacement surgery (n = 47). The human cartilage specimens were macroscopically diagnosed according to the Modified Outerbridge Classification (stage 0, intact cartilage; stage 1, chondral softening and/or blistering with an intact surface; stage 2, superficial ulceration, fibrillation, or fissuring in the cartilage to a depth < 50%; stage 3, deep ulceration, fibrillation, fissuring, or chondral flap in the cartilage to a depth > 50% without any exposed bone; and stage 4, full-thickness wear combined with exposed subchondral bone).[23,24] The clinical characteristics of the patients are included in Table S1. All the mice were purchased from Shanghai SLAC Laboratory Animal (Shanghai, China), and the animal handling and experimental procedures were performed with approval from the Institute of Health Sciences Institutional Animal Care and Use Committee.

Chondrocyte Culture

Human and mouse primary chondrocytes were separately isolated from human and mouse cartilage tissues. Specifically, human cartilage tissues were surgically removed from OA patients under sterile conditions during total knee arthroplasty (TKA) and were subsequently cut into pieces. The diced cartilage was digested with 0.2% collagenase II (Sigma-Aldrich, St. Louis, MO, USA) in serum-free Dulbecco's modified Eagle's medium (DMEM) supplemented with 100 U/mL penicillin and 100 U/mL streptomycin (Invitrogen, Carlsbad, CA, USA) overnight at 37°C in a humidified atmosphere consisting of 5% CO_2 and 95% air. The cells were filtered through a 40-μm cell strainer and washed with sterile phosphate-buffered saline (PBS) before culturing. The cells were maintained in chondrocyte growth medium (ScienCell, CA, USA). Primary mouse chondrocytes were isolated from mice at postnatal day 5 through dissection of the tibial plateaus and femoral condyles as described previously.[60]

Cell Culture and Treatment

The HEK293T (ATCC: CRL-1573) and SW1353 (ATCC: HTB94) cell lines were obtained from the American Type Culture Collection (ATCC, Manassas, VA, USA). The HEK293T cells were maintained in Dulbecco's modified Eagle's medium (DMEM) supplemented with 10% fetal bovine serum (GIBCO, Grand Island, NY, USA), 100 U/mL penicillin, and 100 U/mL streptomycin (Invitrogen, Carlsbad, CA, USA). The SW1353 cells were maintained in Leibovitz's L-15 medium (GIBCO, Grand Island, NY, USA) supplemented with 10% fetal bovine serum (GIBCO, Grand Island, NY, USA), 100 U/mL penicillin, and 100 U/mL streptomycin (Invitrogen, Carlsbad, CA, USA). All the cells were cultured in an incubator at 37°C with 5% CO_2 and determined to be mycoplasma-free.

RNA Extraction and Quantitative Real-Time PCR Analysis

Total RNA from cells and tissues was extracted using the RNAEX reagent (Accurate Biotechnology, Hunan) according to the manufacturer's instructions. For RNase R treatment, 2 mg of total RNA was incubated with or without 3 U/mg RNase R (Epicenter Technologies) for 15 min at 37°C. For circRNA and mRNA analyses, Evo M-MLV RT Premix for qPCR (Accurate Biotechnology, Hunan) and SYBR Green Premix Pro Taq HS qPCR Kit (Accurate Biotechnology, Hunan) were used, and the reactions were subsequently measured using a Roche LightCycler 480II PCR instrument (Basel, Switzerland) in accordance with the manufacturer's recommended protocols. The reactions were normalized to the miRNA housekeeping gene U6 or the mRNA housekeeping gene β-actin. For absolute quantification, standards were generated and diluted. Standard curves between CT values and $\log_{10}$(copy numbers) were constructed. The primers were obtained from RiboBio (Guangzhou, China).

siRNAs, Vector Construction, and Stable Transfection

siRNAs and miR-103a-3p were obtained from Genepharma (Shanghai, China) and transfected into cells with Lipofectamine RNAiMAX (Invitrogen). Human lentivirus-sh-circPDE4D, lentivirus-miR-103a-3p sponge, and lentivirus-miR-103a-3p were purchased from Genepharma (Shanghai, China). The lentiviruses were ultracentrifuged, concentrated, validated, and added to the cell culture medium in the presence of Polybrene (Solarbio, Beijing, China). After infection, the cells were selected with puromycin (GIBCO, Grand Island, NY, USA), and the surviving cells were continuously cultured as stable cells.

Flow Cytometry Assay

Human primary chondrocytes subjected to different treatments were collected using trypsin without EDTA (Thermo Fisher Scientific) and washed twice with PBS. For the apoptosis assay, the cells were stained using an Annexin V-fluorescein isothiocyanate/propidium iodide (FITC/PI) Apoptosis Kit (BD Biosciences, Franklin Lakes, NJ, USA) according to the manufacturer's instructions and then detected using a BD FACS flow cytometer (BD Biosciences). For the cell cycle assay, the cells were fixed overnight in absolute ethanol, washed twice, and incubated with PI/RNase staining buffer (BD Biosciences, Franklin Lakes, NJ, USA), and the specimens were then detected using a BD FACS flow cytometer (BD Biosciences).

RNA Immunoprecipitation

The Ago-RIP assay was conducted using SW1353 cells and the Magna RIP RNA-Binding Protein Immunoprecipitation Kit (Millipore, Bedford, MA, USA). The cells were transfected with NC or miR-103a-3p. Approximately 1×10^7 cells were pelleted and resuspended in an equal volume of RIP lysis buffer plus a protease inhibitor cocktail and RNase inhibitors. The cell lysates (200 μL) were incubated with 5 μg of antibody against Ago2 (Millipore, Billerica, MA, USA), antibody against SNRNP70 (Millipore, Billerica, MA, USA) or control rabbit immunoglobulin G (IgG)-coated beads and mixed by rotation at 4°C overnight. After treatment with proteinase K buffer, the immunoprecipitated RNAs were extracted using the RNeasy MinElute Cleanup Kit (QIAGEN, Duesseldorf, Germany) and reverse transcribed using Prime-Script RT Master Mix (TaKaRa, Tokyo, Japan). The relative expression of circPDE4D was detected by qRT-PCR. U1 snRNA immunoprecipitated by anti-SNRNP70 served as a positive control.

CRISPR-Cas9 Editing

Two guide RNAs targeting both sides of upstream sequences containing all the QREs closing to exon 2 in the flanking introns were designed and transfected into SW1353 cells. After 24 h, cells were treated with 2 ng/mL puromycin and cultured for another 72 h. Monoclonal cells were selected and cultured, followed by Sanger sequencing confirming its editing. Cells with expected editing were selected for further experiments.

Predicted miRNA Targets of circPDE4D

miRNAs that bind to circPDE4D were predicted using the bioinformatics databases TargetScan (http://www.targetscan.org/) and RNAhybrid (https://bibiserv.cebitec.uni-bielefeld.de/rnahybrid/) and the upregulated miRNA sequences in OA cartilage compared with normal tissues identified in our previous study.[14] The overlapping miRNAs were considered reliable miRNA targets of circPDE4D.

Luciferase Assay

The full sequence of circPDE4D was constructed into the circPDE4D-WT reporter plasmid. To obtain the circPDE4D-Mut plasmid, we mutated the predicted binding site of miR-103a-3p in circPDE4D and cloned the constructed full sequence of circPDE4D-Mut into the corresponding reporter plasmid. HEK293T cells were seeded in 96-well plates and cultured to 50%–70% confluence before transfection. For the circPDE4D and miR-103a-3p experiments, 500 ng of circPDE4D-WT or circPDE4D-Mut plasmid were cotransfected with 20 nmol of miR-103a-3p or negative control. For the FGF18 and miR-103a-3p experiments, 500 ng of FGF18 3′UTR-WT or FGF18 3′UTR-Mut plasmid and 20 nmol of miR-103a-3p or negative control were transfected. After a 24-h incubation, a dual-luciferase system was used for the detection of firefly and Renilla luciferase activity. Using Luciferase Assay Reagent II (LAR II; Luciferase Assay Reagent, Promega) and

lysis buffer, the firefly luciferase activities were measured to provide an internal reference, and the Renilla luciferase activities were also measured using Stop & Glo Reagent (Luciferase Assay Reagent, Promega). Finally, the differences between firefly and Renilla luciferase activities were calculated to determine the relative luciferase activity.

Northern Blot

Northern blot analysis was performed using a Northern Blot kit (Ambion, USA). Specifically, total RNA (30 μg) extracted from primary chondrocytes and SW1353 cells was denatured in formaldehyde and then electrophoresed in a 1% agarose-formaldehyde gel. The RNA was transferred onto a nylon membrane (Beyotime, China) and subsequently hybridized with biotin-labeled DNA probes. The bound RNA was detected using a Biotin Chromogenic Detection Kit (Thermo Fisher Scientific), and the membranes were then exposed and analyzed using Image Lab software (Bio-Rad, USA).

Western Blotting

For total protein extraction, primary human chondrocytes and SW1353 cells were lysed in RIPA buffer (Fudebio, Hangzhou, China) containing protease inhibitor cocktails and phosphatase inhibitors (Fudebio, Hangzhou, China). The protein concentrations were determined using a bicinchoninic acid protein assay kit (Thermo Fisher Scientific). Equivalent amounts of protein were separated by SDS-PAGE and transferred onto polyvinylidene fluoride membranes (Merck KGaA). After incubation with a high-affinity anti-MMP13 antibody (1:1,000, Abcam), anti-MMP3 antibody (1:1,000, Abcam), anti-ADAMTS4 antibody (1:1,000, Abcam), anti-ADAMTS5 antibody (1:1,000, Abcam), anti-Col2a1 antibody (1:1,000, Proteintech), anti-Aggrecan antibody (1:100, Abcam), anti-FGF18 antibody (1:1000, Proteintech), anti-FGFR3 (1:1,000, Abcam), anti-$FGFR3^{p\text{-}Tyr724}$ (1:1,000, Abcam), anti-ERK/2 (1:1,000, Abcam), anti-$ERK1/2^{p\text{-}Thr202/204}$ (1:1,000, Abcam) anti-cleaved-Caspase 3 (1:1,000, Abcam), anti-Caspase 3 (1:1,000, Abcam) anti-Bcl-2 (1:1,000, Abcam), anti-Bax (1:1,000, Abcam), or anti-β-actin antibody (1:2,000; Cell Signaling Technology, USA), the membranes were incubated with a horseradish peroxidase (HRP)-conjugated secondary antibody (FDM007 and FDR007, Fudebio, Hangzhou, China). After washing, signals were detected using an enhanced chemiluminescence kit (FD8030, Fudebio, Hangzhou, China). Primary antibody dilution buffer was purchased from Dalian Meilun Biotechnology (MB9881, Dalian, China).

FISH

CY3-labeled circPDE4D probes and Alexa Fluor 488-labeled miR-103a-3p probes were designed and synthesized by RiboBio (Guangzhou, China). The cell nuclei were labeled with DAPI (4′,6-diamidino-2-phenylindole) (Sigma-Aldrich, St. Louis, MO, USA). The probe signals were determined using the FISH Kit (RiboBio, Guangzhou, China) according to the manufacturer's guidelines. Images were obtained using a fluorescence microscope (Eclipse E600; Nikon Corporation, Tokyo, Japan).

Articular Injection in an Animal Model

Articular injections were performed using 10 μL microsyringe with 34 G needle (Hamilton, Switzerland). For AAVs injection, AAV circPDE4D-WT and the corresponding Mut were constructed and packaged into pHBAAV-CMV-circRNA-EF1-ZsGreen by HANBIO (Shanghai, China). 2 weeks after the DMM surgery, the mice were randomly divided into three groups (DMM, circPDE4D injection, and circPDE4D-mut injection), and 10 μL of solution containing experimental or control virus (approximately 1 × 10E12 vg/mL) overexpressing circPDE4D was then slowly injected into the knees. The injection procedure was repeated after 2 weeks. For RNA oligo injection, si- mmu-circPDE4D and miR-103a-3p antagomiR were modified with 5′ Cholesteroi and 2′OME in order to enhance the permeability and stability *in vivo*. 0.4 OD siRNA and antagomiR together with lipofectamine 3000 were injected once a week until animal was sacrificed. FISH of knee specimens after sacrifice was performed to confirm the success of injection.

Animal Praxeology Experiments

For the rotarod assay, the mice were placed onto the rotarod (Ugo Basile) at a constant speed for training. After training, the mice were placed onto an accelerating rotarod, and the time spent on the rotarod was determined by the duration of time that each mouse stayed on top of the rod until the first failure. Each trial consisted of a maximum time of 5 min. The mice were allowed an inter-trial rest interval of 30 min. For the hot plate test, mice belonging to each group were placed on a hot plate (Columbus Instruments) at 55°C. The time to response (jumping or licking hind legs) for the latency period was recorded. The rotarod and hot plate tests were evaluated by two observers who were blinded to the experimental design.

Histological Analyses

Human and mouse cartilage specimens were fixed in 4% paraformaldehyde and decalcified for paraffin embedding, and the OA severity was quantified using the OARSI histopathology grading system[61] and Mankin score[62] by two blinded independent observers. The sections were stained with Safranin-O/Fast green (Solarbio, Beijing, China) or Alcian blue (Solarbio, Beijing, China) according to standard protocols. The immunohistochemistry and immunofluorescence procedures have been previously described.[14,63]

Statistical Analysis

The statistical analyses were performed with SPSS v22.0 software. The data are presented as the means ± SDs. The distribution of the data was tested with the Shapiro-Wilk test. The equality of variances was tested using Levene's test. The statistical significance ($^*p < 0.05$ and $^{**}p < 0.01$) was determined by unpaired two-tailed t tests or one-way ANOVA followed by the Bonferroni test unless indicated otherwise.

SUPPLEMENTAL INFORMATION

Supplemental Information can be found online at https://doi.org/10.1016/j.ymthe.2020.09.002.

AUTHOR CONTRIBUTIONS

Y.W., Z.H., and W.X. contributed equally to this work. Y.W., Z.H., W.X., Junxin Chen, and Q.W. conducted the experiments. Jiaxin Chen, Y.W., W.N., Z.M., and J.W. analyzed the data. S.S. and S.F. designed the experiments. Y.W., J.L., Z.X., and C.C. wrote the paper.

CONFLICTS OF INTEREST

The authors declare no competing interests.

ACKNOWLEDGMENTS

This work was supported by National Key R&D Program of China (number 2018YFC1105200), the Key Research and Development Plan in Zhejiang Province (number 2018C03060), National Natural Science Foundation of China (grant numbers 81772387 and 81802680), Major Projects for Industry-University-Research Collaborative Innovation of Science, and Technology Plan of Guangzhou City (grant number 201604020095).

REFERENCES

1. Bijlsma, J.W., Berenbaum, F., and Lafeber, F.P. (2011). Osteoarthritis: an update with relevance for clinical practice. Lancet *377*, 2115–2126.
2. Hunter, D.J., Schofield, D., and Callander, E. (2014). The individual and socioeconomic impact of osteoarthritis. Nat. Rev. Rheumatol. *10*, 437–441.
3. Mouw, J.K., Ou, G., and Weaver, V.M. (2014). Extracellular matrix assembly: a multiscale deconstruction. Nat. Rev. Mol. Cell Biol. *15*, 771–785.
4. Troeberg, L., and Nagase, H. (2012). Proteases involved in cartilage matrix degradation in osteoarthritis. Biochim. Biophys. Acta *1824*, 133–145.
5. Hunter, D.J., and Bierma-Zeinstra, S. (2019). Osteoarthritis. Lancet *393*, 1745–1759.
6. Carr, A.J., Robertsson, O., Graves, S., Price, A.J., Arden, N.K., Judge, A., and Beard, D.J. (2012). Knee replacement. Lancet *379*, 1331–1340.
7. Kristensen, L.S., Andersen, M.S., Stagsted, L.V.W., Ebbesen, K.K., Hansen, T.B., and Kjems, J. (2019). The biogenesis, biology and characterization of circular RNAs. Nat. Rev. Genet. *20*, 675–691.
8. Ivanov, A., Memczak, S., Wyler, E., Torti, F., Porath, H.T., Orejuela, M.R., Piechotta, M., Levanon, E.Y., Landthaler, M., Dieterich, C., and Rajewsky, N. (2015). Analysis of intron sequences reveals hallmarks of circular RNA biogenesis in animals. Cell Rep. *10*, 170–177.
9. Zhang, X.O., Wang, H.B., Zhang, Y., Lu, X., Chen, L.L., and Yang, L. (2014). Complementary sequence-mediated exon circularization. Cell *159*, 134–147.
10. Conn, S.J., Pillman, K.A., Toubia, J., Conn, V.M., Salmanidis, M., Phillips, C.A., Roslan, S., Schreiber, A.W., Gregory, P.A., and Goodall, G.J. (2015). The RNA binding protein quaking regulates formation of circRNAs. Cell *160*, 1125–1134.
11. Rybak-Wolf, A., Stottmeister, C., Glažar, P., Jens, M., Pino, N., Giusti, S., Hanan, M., Behm, M., Bartok, O., Ashwal-Fluss, R., et al. (2015). Circular RNAs in the Mammalian Brain Are Highly Abundant, Conserved, and Dynamically Expressed. Mol. Cell *58*, 870–885.
12. Venø, M.T., Hansen, T.B., Venø, S.T., Clausen, B.H., Grebing, M., Finsen, B., Holm, I.E., and Kjems, J. (2015). Spatio-temporal regulation of circular RNA expression during porcine embryonic brain development. Genome Biol. *16*, 245.
13. Liu, G., Huang, K., Jie, Z., Wu, Y., Chen, J., Chen, Z., Fang, X., and Shen, S. (2018). CircFAT1 sponges miR-375 to promote the expression of Yes-associated protein 1 in osteosarcoma cells. Mol. Cancer *17*, 170.
14. Shen, S., Wu, Y., Chen, J., Xie, Z., Huang, K., Wang, G., Yang, Y., Ni, W., Chen, Z., Shi, P., et al. (2019). CircSERPINE2 protects against osteoarthritis by targeting miR-1271 and ETS-related gene. Ann. Rheum. Dis. *78*, 826–836.
15. Wu, Y., Xie, Z., Chen, J., Chen, J., Ni, W., Ma, Y., Huang, K., Wang, G., Wang, J., Ma, J., et al. (2019). Circular RNA circTADA2A promotes osteosarcoma progression and metastasis by sponging miR-203a-3p and regulating CREB3 expression. Mol. Cancer *18*, 73.
16. Memczak, S., Jens, M., Elefsinioti, A., Torti, F., Krueger, J., Rybak, A., Maier, L., Mackowiak, S.D., Gregersen, L.H., Munschauer, M., et al. (2013). Circular RNAs are a large class of animal RNAs with regulatory potency. Nature *495*, 333–338.
17. Ashwal-Fluss, R., Meyer, M., Pamudurti, N.R., Ivanov, A., Bartok, O., Hanan, M., Evantal, N., Memczak, S., Rajewsky, N., and Kadener, S. (2014). circRNA biogenesis competes with pre-mRNA splicing. Mol. Cell *56*, 55–66.
18. Li, Z., Huang, C., Bao, C., Chen, L., Lin, M., Wang, X., Zhong, G., Yu, B., Hu, W., Dai, L., et al. (2015). Exon-intron circular RNAs regulate transcription in the nucleus. Nat. Struct. Mol. Biol. *22*, 256–264.
19. Du, W.W., Yang, W., Liu, E., Yang, Z., Dhaliwal, P., and Yang, B.B. (2016). Foxo3 circular RNA retards cell cycle progression via forming ternary complexes with p21 and CDK2. Nucleic Acids Res. *44*, 2846–2858.
20. Zeng, Y., Du, W.W., Wu, Y., Yang, Z., Awan, F.M., Li, X., Yang, W., Zhang, C., Yang, Q., Yee, A., et al. (2017). A Circular RNA Binds To and Activates AKT Phosphorylation and Nuclear Localization Reducing Apoptosis and Enhancing Cardiac Repair. Theranostics *7*, 3842–3855.
21. Pamudurti, N.R., Bartok, O., Jens, M., Ashwal-Fluss, R., Stottmeister, C., Ruhe, L., Hanan, M., Wyler, E., Perez-Hernandez, D., Ramberger, E., et al. (2017). Translation of CircRNAs. Mol. Cell *66*, 9–21.
22. Zhang, M., Zhao, K., Xu, X., Yang, Y., Yan, S., Wei, P., Liu, H., Xu, J., Xiao, F., Zhou, H., et al. (2018). A peptide encoded by circular form of LINC-PINT suppresses oncogenic transcriptional elongation in glioblastoma. Nat. Commun. *9*, 4475.
23. Cameron, M.L., Briggs, K.K., and Steadman, J.R. (2003). Reproducibility and reliability of the outerbridge classification for grading chondral lesions of the knee arthroscopically. Am. J. Sports Med. *31*, 83–86.
24. Zhang, Q., Ji, Q., Wang, X., Kang, L., Fu, Y., Yin, Y., Li, Z., Liu, Y., Xu, X., and Wang, Y. (2015). SOX9 is a regulator of ADAMTSs-induced cartilage degeneration at the early stage of human osteoarthritis. Osteoarthritis Cartilage *23*, 2259–2268.
25. Greene, M.A., and Loeser, R.F. (2015). Aging-related inflammation in osteoarthritis. Osteoarthritis Cartilage *23*, 1966–1971.
26. Robinson, W.H., Lepus, C.M., Wang, Q., Raghu, H., Mao, R., Lindstrom, T.M., and Sokolove, J. (2016). Low-grade inflammation as a key mediator of the pathogenesis of osteoarthritis. Nat. Rev. Rheumatol. *12*, 580–592.
27. Wang, X., Hunter, D., Xu, J., and Ding, C. (2015). Metabolic triggered inflammation in osteoarthritis. Osteoarthritis Cartilage *23*, 22–30.
28. Hansen, T.B., Jensen, T.I., Clausen, B.H., Bramsen, J.B., Finsen, B., Damgaard, C.K., and Kjems, J. (2013). Natural RNA circles function as efficient microRNA sponges. Nature *495*, 384–388.
29. Attur, M., Krasnokutsky, S., Statnikov, A., Samuels, J., Li, Z., Friese, O., Hellio Le Graverand-Gastineau, M.P., Rybak, L., Kraus, V.B., Jordan, J.M., et al. (2015). Low-grade inflammation in symptomatic knee osteoarthritis: prognostic value of inflammatory plasma lipids and peripheral blood leukocyte biomarkers. Arthritis Rheumatol. *67*, 2905–2915.
30. June, R.K., Liu-Bryan, R., Long, F., and Griffin, T.M. (2016). Emerging role of metabolic signaling in synovial joint remodeling and osteoarthritis. J. Orthop. Res. *34*, 2048–2058.
31. Zhuo, Q., Yang, W., Chen, J., and Wang, Y. (2012). Metabolic syndrome meets osteoarthritis. Nat. Rev. Rheumatol. *8*, 729–737.
32. Blanco, F.J., Rego, I., and Ruiz-Romero, C. (2011). The role of mitochondria in osteoarthritis. Nat. Rev. Rheumatol. *7*, 161–169.
33. Scott, J.L., Gabrielides, C., Davidson, R.K., Swingler, T.E., Clark, I.M., Wallis, G.A., Boot-Handford, R.P., Kirkwood, T.B., Taylor, R.W., and Young, D.A. (2010). Superoxide dismutase downregulation in osteoarthritis progression and end-stage disease. Ann. Rheum. Dis. *69*, 1502–1510.
34. Aktaş, T., Avşar Ilık, İ., Maticzka, D., Bhardwaj, V., Pessoa Rodrigues, C., Mittler, G., Manke, T., Backofen, R., and Akhtar, A. (2017). DHX9 suppresses RNA processing defects originating from the Alu invasion of the human genome. Nature *544*, 115–119.

35. Kim, D.D., Kim, T.T., Walsh, T., Kobayashi, Y., Matise, T.C., Buyske, S., and Gabriel, A. (2004). Widespread RNA editing of embedded alu elements in the human transcriptome. Genome Res. *14*, 1719–1725.

36. Galarneau, A., and Richard, S. (2005). Target RNA motif and target mRNAs of the Quaking STAR protein. Nat. Struct. Mol. Biol. *12*, 691–698.

37. Yu, M., Xue, Y., Zheng, J., Liu, X., Yu, H., Liu, L., Li, Z., and Liu, Y. (2017). Linc00152 promotes malignant progression of glioma stem cells by regulating miR-103a-3p/FEZF1/CDC25A pathway. Mol. Cancer *16*, 110.

38. Zhong, Z., Lv, M., and Chen, J. (2016). Screening differential circular RNA expression profiles reveals the regulatory role of circTCF25-miR-103a-3p/miR-107-CDK6 pathway in bladder carcinoma. Sci. Rep. *6*, 30919.

39. Davidson, D., Blanc, A., Filion, D., Wang, H., Plut, P., Pfeffer, G., Buschmann, M.D., and Henderson, J.E. (2005). Fibroblast growth factor (FGF) 18 signals through FGF receptor 3 to promote chondrogenesis. J. Biol. Chem. *280*, 20509–20515.

40. Liu, Z., Lavine, K.J., Hung, I.H., and Ornitz, D.M. (2007). FGF18 is required for early chondrocyte proliferation, hypertrophy and vascular invasion of the growth plate. Dev. Biol. *302*, 80–91.

41. Chen, T., Gong, W., Tian, H., Wang, H., Chu, S., Ma, J., Yang, H., Cheng, J., Liu, M., Li, X., and Jiang, C. (2017). Fibroblast growth factor 18 promotes proliferation and migration of H460 cells via the ERK and p38 signaling pathways. Oncol. Rep. *37*, 1235–1242.

42. Zhang, J., Zhou, Y., Huang, T., Wu, F., Pan, Y., Dong, Y., Wang, Y., Chan, A.K.Y., Liu, L., Kwan, J.S.H., et al. (2019). FGF18, a prominent player in FGF signaling, promotes gastric tumorigenesis through autocrine manner and is negatively regulated by miR-590-5p. Oncogene *38*, 33–46.

43. Liu-Bryan, R., and Terkeltaub, R. (2015). Emerging regulators of the inflammatory process in osteoarthritis. Nat. Rev. Rheumatol. *11*, 35–44.

44. Wang, Q., Rozelle, A.L., Lepus, C.M., Scanzello, C.R., Song, J.J., Larsen, D.M., Crish, J.F., Bebek, G., Ritter, S.Y., Lindstrom, T.M., et al. (2011). Identification of a central role for complement in osteoarthritis. Nat. Med. *17*, 1674–1679.

45. Yang, S., Kim, J., Ryu, J.H., Oh, H., Chun, C.H., Kim, B.J., Min, B.H., and Chun, J.S. (2010). Hypoxia-inducible factor-2alpha is a catabolic regulator of osteoarthritic cartilage destruction. Nat. Med. *16*, 687–693.

46. Dichgans, M. (2007). Genetics of ischaemic stroke. Lancet Neurol. *6*, 149–161.

47. Gretarsdottir, S., Thorleifsson, G., Reynisdottir, S.T., Manolescu, A., Jonsdottir, S., Jonsdottir, T., Gudmundsdottir, T., Bjarnadottir, S.M., Einarsson, O.B., Gudjonsdottir, H.M., et al. (2003). The gene encoding phosphodiesterase 4D confers risk of ischemic stroke. Nat. Genet. *35*, 131–138.

48. Mishra, R.R., Belder, N., Ansari, S.A., Kayhan, M., Bal, H., Raza, U., Ersan, P.G., Tokat, Ü.M., Eyüpoğlu, E., Saatci, Ö., et al. (2018). Reactivation of cAMP Pathway by PDE4D Inhibition Represents a Novel Druggable Axis for Overcoming Tamoxifen Resistance in ER-positive Breast Cancer. Clin. Cancer Res. *24*, 1987–2001.

49. Hwang, H.S., and Kim, H.A. (2015). Chondrocyte Apoptosis in the Pathogenesis of Osteoarthritis. Int. J. Mol. Sci. *16*, 26035–26054.

50. Ohbayashi, N., Shibayama, M., Kurotaki, Y., Imanishi, M., Fujimori, T., Itoh, N., and Takada, S. (2002). FGF18 is required for normal cell proliferation and differentiation during osteogenesis and chondrogenesis. Genes Dev. *16*, 870–879.

51. Yao, X., Zhang, J., Jing, X., Ye, Y., Guo, J., Sun, K., and Guo, F. (2019). Fibroblast growth factor 18 exerts anti-osteoarthritic effects through PI3K-AKT signaling and mitochondrial fusion and fission. Pharmacol. Res. *139*, 314–324.

52. Cinque, L., Forrester, A., Bartolomeo, R., Svelto, M., Venditti, R., Montefusco, S., Polishchuk, E., Nusco, E., Rossi, A., Medina, D.L., et al. (2015). FGF signalling regulates bone growth through autophagy. Nature *528*, 272–275.

53. Tachmazidou, I., Hatzikotoulas, K., Southam, L., Esparza-Gordillo, J., Haberland, V., Zheng, J., Johnson, T., Koprulu, M., Zengini, E., Steinberg, J., et al.; arcOGEN Consortium (2019). Identification of new therapeutic targets for osteoarthritis through genome-wide analyses of UK Biobank data. Nat. Genet. *51*, 230–236.

54. Carli, A., Gao, C., Khayyat-Kholghi, M., Li, A., Wang, H., Ladel, C., Harvey, E.J., and Henderson, J.E. (2012). FGF18 augments osseointegration of intra-medullary implants in osteopenic FGFR3(-/-) mice. Eur. Cell. Mater. *24*, 107–116, discussion 116–117.

55. Ellman, M.B., Yan, D., Ahmadinia, K., Chen, D., An, H.S., and Im, H.J. (2013). Fibroblast growth factor control of cartilage homeostasis. J. Cell. Biochem. *114*, 735–742.

56. Gigout, A., Guehring, H., Froemel, D., Meurer, A., Ladel, C., Reker, D., Bay-Jensen, A.C., Karsdal, M.A., and Lindemann, S. (2017). Sprifermin (rhFGF18) enables proliferation of chondrocytes producing a hyaline cartilage matrix. Osteoarthritis Cartilage *25*, 1858–1867.

57. Kumar, M.S., Armenteros-Monterroso, E., East, P., Chakravorty, P., Matthews, N., Winslow, M.M., and Downward, J. (2014). HMGA2 functions as a competing endogenous RNA to promote lung cancer progression. Nature *505*, 212–217.

58. Tay, Y., Rinn, J., and Pandolfi, P.P. (2014). The multilayered complexity of ceRNA crosstalk and competition. Nature *505*, 344–352.

59. Salmena, L., Poliseno, L., Tay, Y., Kats, L., and Pandolfi, P.P. (2011). A ceRNA hypothesis: the Rosetta Stone of a hidden RNA language? Cell *146*, 353–358.

60. Gosset, M., Berenbaum, F., Thirion, S., and Jacques, C. (2008). Primary culture and phenotyping of murine chondrocytes. Nat. Protoc. *3*, 1253–1260.

61. Pritzker, K.P., Gay, S., Jimenez, S.A., Ostergaard, K., Pelletier, J.P., Revell, P.A., Salter, D., and van den Berg, W.B. (2006). Osteoarthritis cartilage histopathology: grading and staging. Osteoarthritis Cartilage *14*, 13–29.

62. van der Sluijs, J.A., Geesink, R.G., van der Linden, A.J., Bulstra, S.K., Kuyer, R., and Drukker, J. (1992). The reliability of the Mankin score for osteoarthritis. J. Orthop. Res. *10*, 58–61.

63. Shen, S., Huang, K., Wu, Y., Ma, Y., Wang, J., Qin, F., and Ma, J. (2017). A miR-135b-TAZ positive feedback loop promotes epithelial-mesenchymal transition (EMT) and tumorigenesis in osteosarcoma. Cancer Lett. *407*, 32–44.

YMTHE, Volume *29*

Supplemental Information

Circular RNA circPDE4D Protects against Osteoarthritis by Binding to miR-103a-3p and Regulating FGF18

Yizheng Wu, Zhenghua Hong, Wenbin Xu, Junxin Chen, Qingxin Wang, Jiaxin Chen, Weiyu Ni, Zixuan Mei, Ziang Xie, Yan Ma, Jiying Wang, Jianhong Lu, Chao Chen, Shunwu Fan, and Shuying Shen

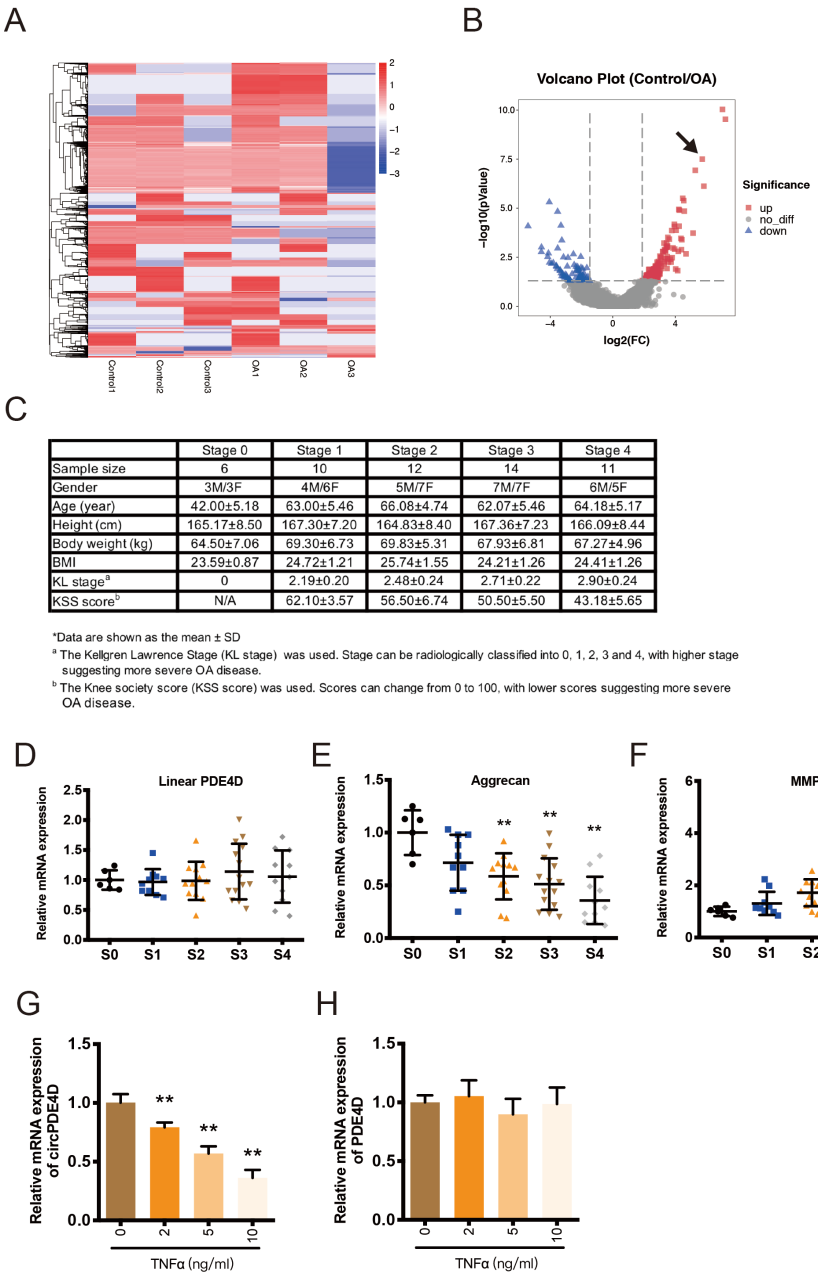

	Stage 0	Stage 1	Stage 2	Stage 3	Stage 4
Sample size	6	10	12	14	11
Gender	3M/3F	4M/6F	5M/7F	7M/7F	6M/5F
Age (year)	42.00±5.18	63.00±5.46	66.08±4.74	62.07±5.46	64.18±5.17
Height (cm)	165.17±8.50	167.30±7.20	164.83±8.40	167.36±7.23	166.09±8.44
Body weight (kg)	64.50±7.06	69.30±6.73	69.83±5.31	67.93±6.81	67.27±4.96
BMI	23.59±0.87	24.72±1.21	25.74±1.55	24.21±1.26	24.41±1.26
KL stage[a]	0	2.19±0.20	2.48±0.24	2.71±0.22	2.90±0.24
KSS score[b]	N/A	62.10±3.57	56.50±6.74	50.50±5.50	43.18±5.65

*Data are shown as the mean ± SD

[a] The Kellgren Lawrence Stage (KL stage) was used. Stage can be radiologically classified into 0, 1, 2, 3 and 4, with higher stage suggesting more severe OA disease.

[b] The Knee society score (KSS score) was used. Scores can change from 0 to 100, with lower scores suggesting more severe OA disease.

Supplementary Figure 1. Information on clinical cartilage specimens.

(A-B) Heatmap (A) and corresponding volcano plot (B) of differentially expressed circRNAs between control and OA cartilage specimens from our previous study. circPDE4D is indicated by a black arrow. The raw data are available on the NCBI SRA database (SRA accession number: PRJNA516555). (C) Information on the human specimens, including size, gender, age, height, body weight, BMI, KL stage and KSS score. (D-F) Expression of linear PDE4D, Aggrecan and MMP3 in 53 human cartilage specimens obtained by qRT-PCR analysis. (G-H) The expression of circPDE4D and linear PDE4D in human primary chondrocytes (HCs) stimulated with TNFα at concentrations of 0, 2, 5, or 10 ng/ml for 24 h was determined by qRT-PCR. The data were obtained from three independent donors (presented as the means ± SDs) (G-H) (*P<0.05 and **P<0.01 vs the control or indicated group). The data were analyzed by one-way ANOVA followed by the Bonferroni test (D-F) or two-tailed t-tests (G-H).

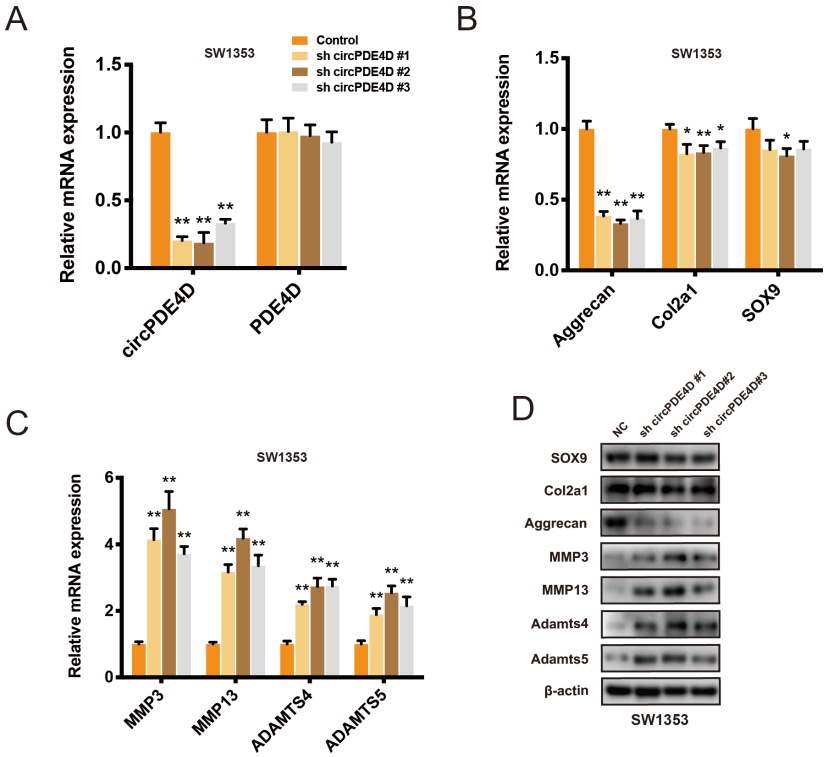

Supplementary Figure 2. The knockdown of circPDE4D induces matrix degradation in SW1353 cells.

(A) SW1353 cells were transfected with sh-circPDE4D #1, #2, #3 or NC and then used for qRT-PCR analysis. The histogram demonstrates the changes in the expression of circPDE4D and linear PDE4D. (B-C) SW1353 cells were stably transfected with sh-circPDE4D #1, #2, #3 or negative control, and the expression of Col2a1, Aggrecan, SOX9, MMP3, MMP13, ADAMTS4, and ADAMTS5 was evaluated by qRT-PCR. (D) The protein levels of SOX9, Col2a1, Aggrecan, MMP3, MMP13, ADAMTS4, and ADAMTS5 in stable SW1353 cells were evaluated by Western blotting. The data were obtained from three independent experiments (presented as the means ± SDs) (A-C) or were representative of three independent experiments with similar results (D). (*P<0.05 and **P<0.01 vs the control or indicated group) The data were analyzed by two-tailed t-tests (A-C).

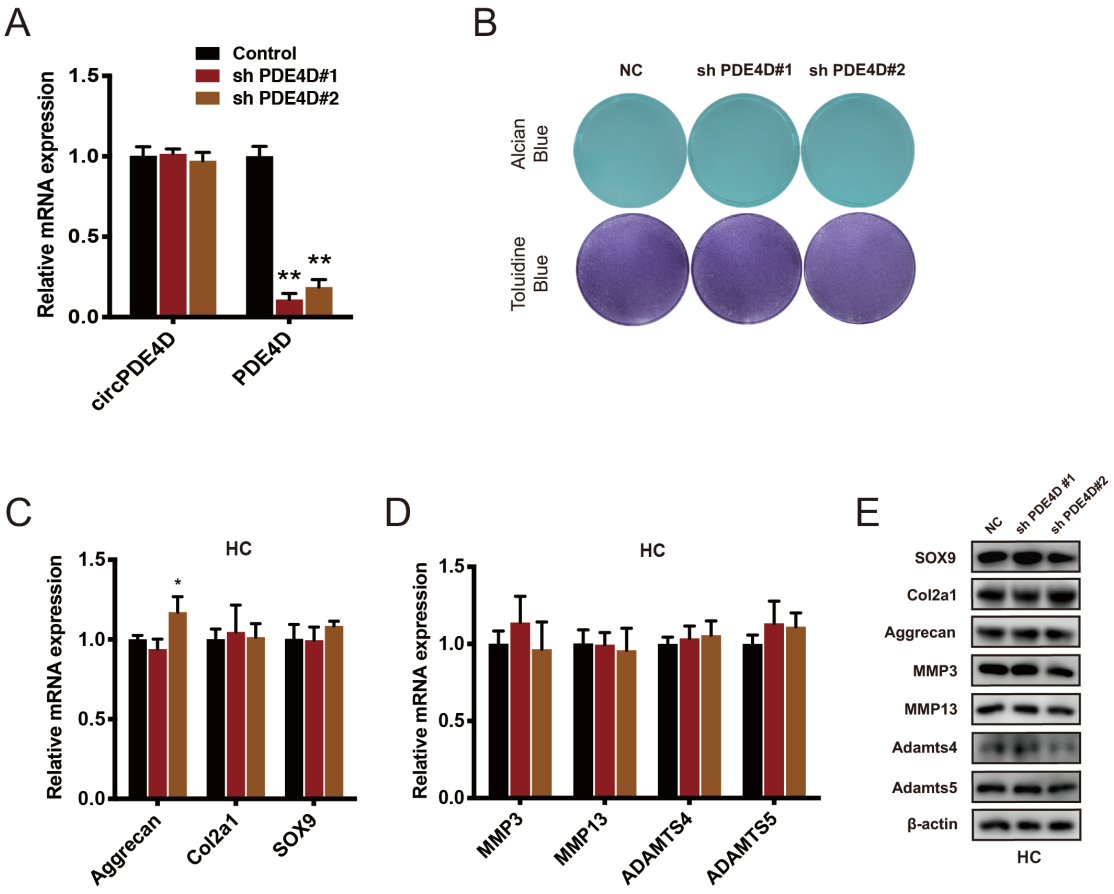

Supplementary Figure 3. Linear PDE4D is not related to matrix degradation. (A) HCs were stably transfected with sh-PDE4D #1, #2 or negative control. The histogram demonstrates the changes in the expression of circPDE4D and PDE4D. (B) The accumulation of proteoglycans was measured by Alcian blue and toluidine blue staining. (C-E) The expression of Col2a1, Aggrecan, SOX9, MMP3, MMP13, ADAMTS4, and ADAMTS5 at the mRNA and protein levels in HCs was evaluated by qRT-PCR and Western blotting. The data were obtained from three independent donors (presented as the means ± SDs) (A, C and D) or were representative of three independent experiments with similar results (B and E). (*P<0.05 and **P<0.01 vs the control or indicated group) The data were analyzed by two-tailed t-tests (A, C and D).

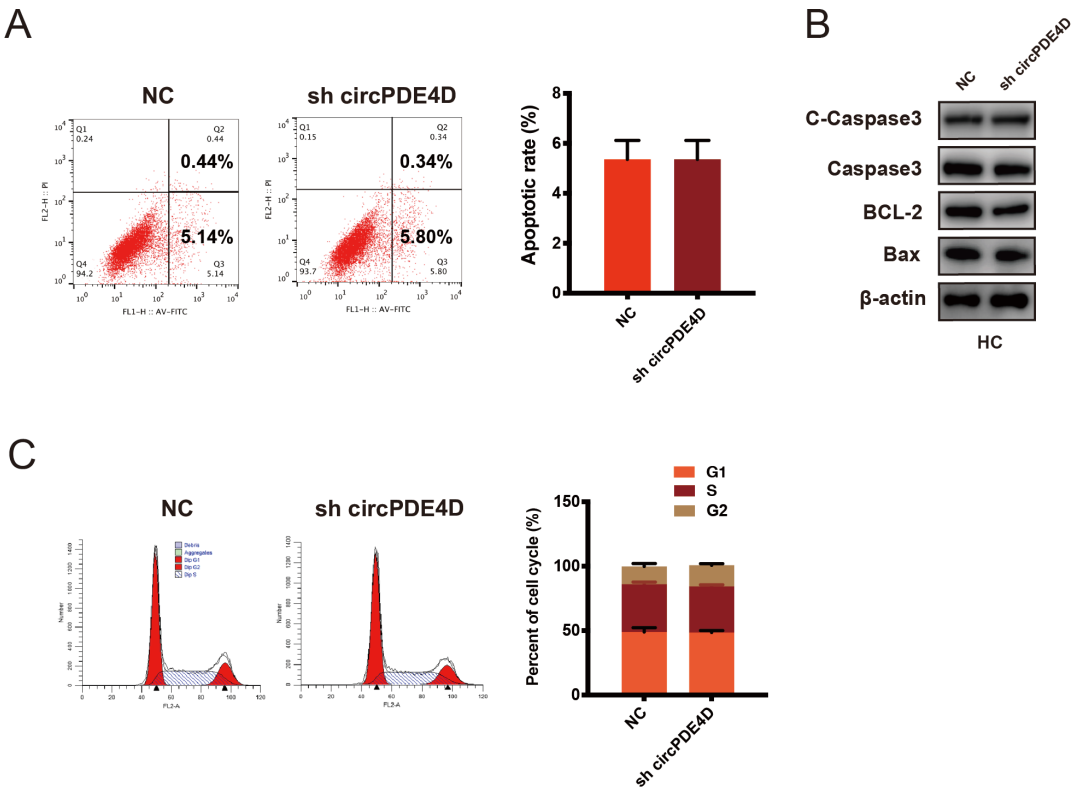

Supplementary Figure 4. circPDE4D is not related to apoptosis or the cell cycle. (A) Stable HCs were collected, stained with Annexin V-FITC and PI, and subjected to flow cytometry detection. Representative images and histograms are shown. (B) The expression of apoptosis-associated proteins (cleaved-Caspase 3, Caspase 3, BCL-2 and Bax) was evaluated by Western blotting. (C) The proportions of circPDE4D-knockdown HCs and their matched control cells at different phases of the cell cycle (G1, S and G2) were evaluated by flow cytometry. The data were obtained from three independent experiments with three independent donors (presented as the means ± SDs) (A and C) or were representative of three independent experiments with similar results (B). (*P<0.05 and **P<0.01 vs the control or indicated group). The data were analyzed by two-tailed t-tests (A and C).

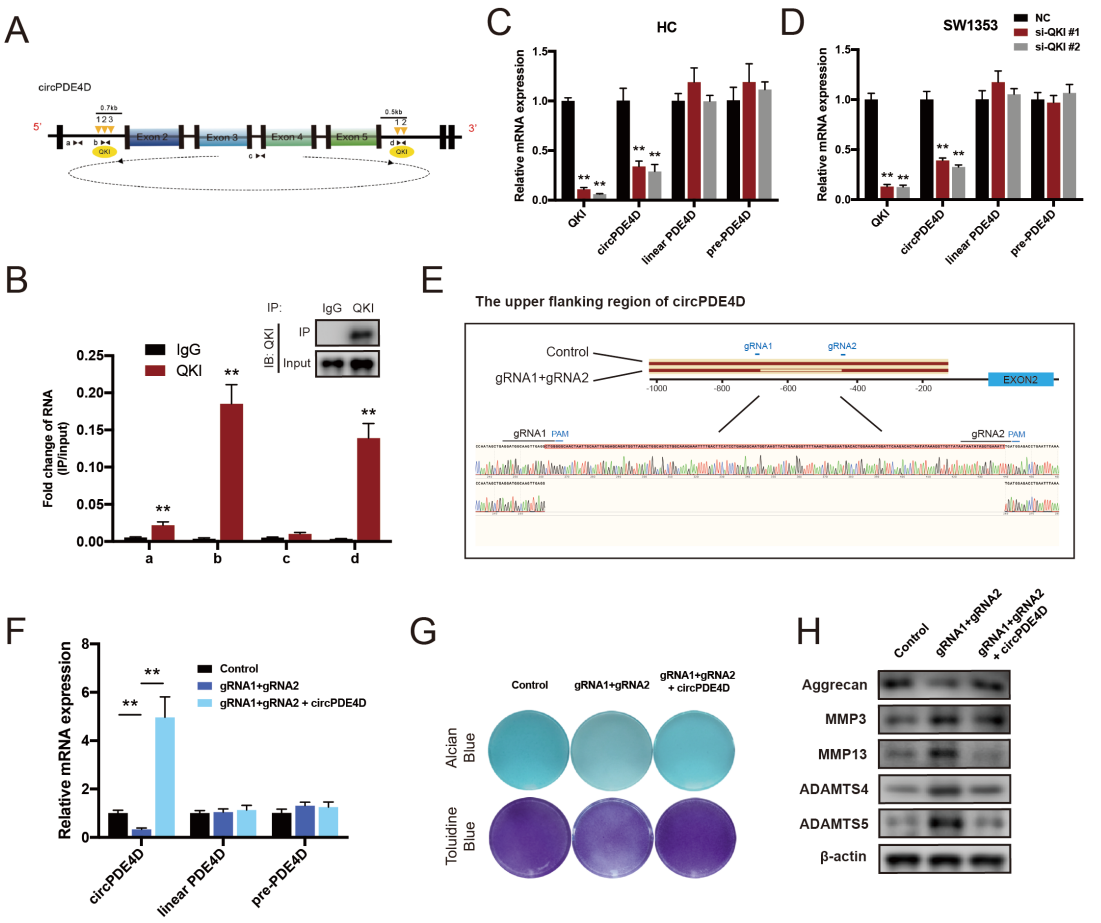

Supplementary Figure 5. Blocking the circPDE4D signal induces OA phenotypes in SW1353 cells.

(A) Schematic diagram of QKI response elements (QREs) in the flanking regions of circPDE4D. a, b, c and d respectively represent the primers in the remote region, upperstream flanking, splicing junction and downstream flanking region of circPDE4D. (B) The corresponding mRNAs in (A) were pulled by QKI and IgG and detected by RNA immunoprecipitation assay followed by qRT-PCR. (C-D) The relative mRNA levels of circPDE4D, linear PDE4D and pre-PDE4D after QKI knockdown were detected by qRT-PCR. (E) Sanger sequencing confirming the gene editing in the upper flanking region containing all the QREs by CRISPR/Cas9. (F) qRT-PCR indicated the expression of circPDE4D, linear PDE4D and pre-PDE4D after CRISPR/Cas9 or co-overexpression of circPDE4D. (G) Alcian blue and toluidine blue staining in the corresponding treatments were measured in SW1353. (H) The protein levels of Aggrecan, MMP3, MMP13, ADAMTS4 and ADAMTS5 were evaluated by Western blotting. The data were obtained from three independent experiments (presented as the means ± SDs) (B-D and F) or were representative of three independent experiments with similar results (G and H). (*P<0.05 and **P<0.01 vs the control or indicated group). The data were analyzed by two-tailed t-tests (B-D and F).

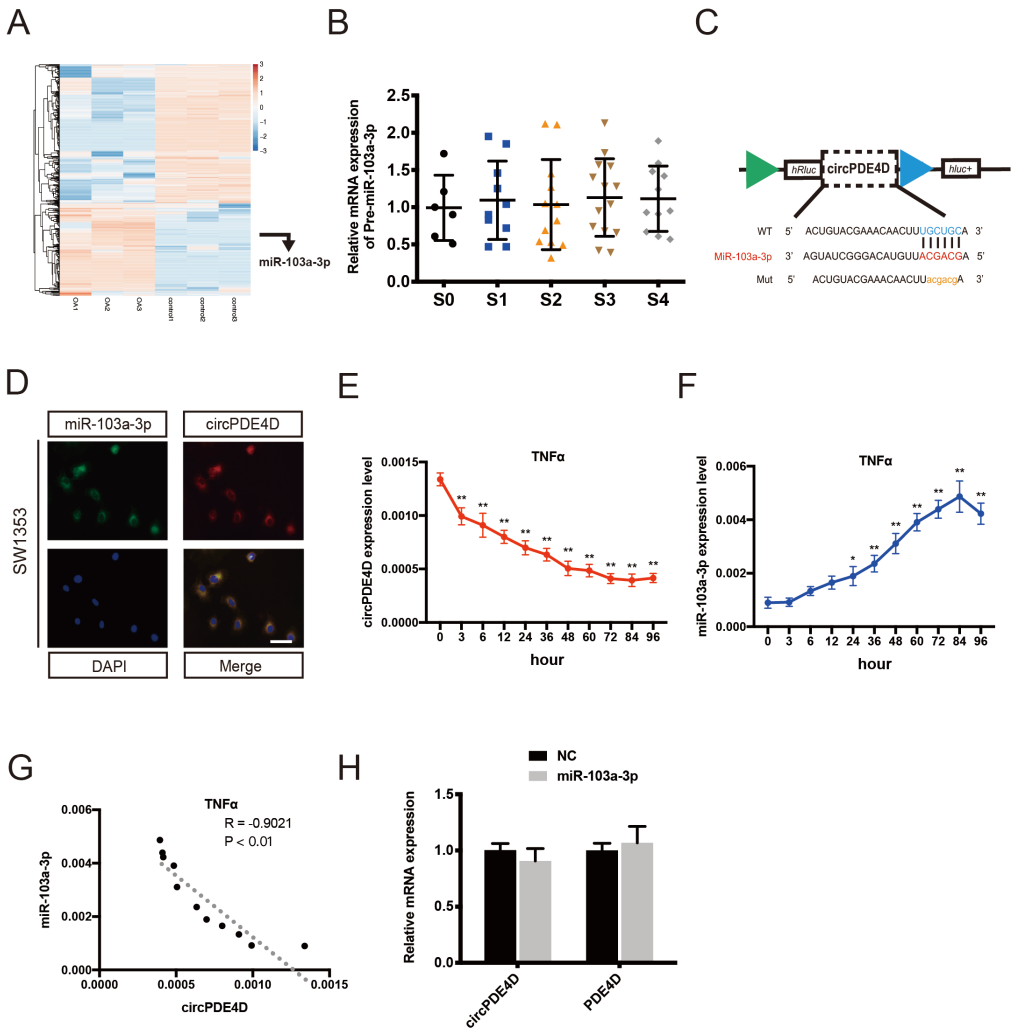

Supplementary Figure 6. miR-103a-3p expression and the correlation analysis. (A) miRNA sequencing of OA and normal cartilage specimens in our previously reported study. The raw data can be found at the NCBI SRA database (SRA accession number: PRJNA516556). (B) Abundances of pre-miR-103a-3p in clinical cartilage tissues. (C) Schematic illustration demonstrating the complementary miR-103a-3p seed sequence with circPDE4D. Lower letters indicate mutated nucleotides. (D) FISH images showing the colocalization of circPDE4D and miR-103a-3p in SW1353 cells. miR-103a-3p probes were labeled with Alexa Fluor 488. The circPDE4D probes were labeled with CY3. Nuclei were stained with DAPI. Scale bar: 20 μm. (E-F) Expression of circPDE4D (normalized to β-actin) and miR-103-3p (normalized to U6) after TNFα stimulation for different time points. (G) Pearson correlation analysis of circPDE4D and miR-103a-3p after TNFα stimulation for different time points (Pearson r=–0.9021; P<0.01). (H) The mRNA expression of circPDE4D and PDE4D after miR-103a-3p overexpression was detected by qRT-PCR. The data were obtained from three independent experiments with three independent donors (presented as the means ± SDs) (E, F and H) or were representative of three independent experiments with similar results (D). (*P<0.05 and **P<0.01 vs the control or indicated group). The data were analyzed by one-way ANOVA followed by the Bonferroni test (B, E and F) or two-tailed t-test (H).

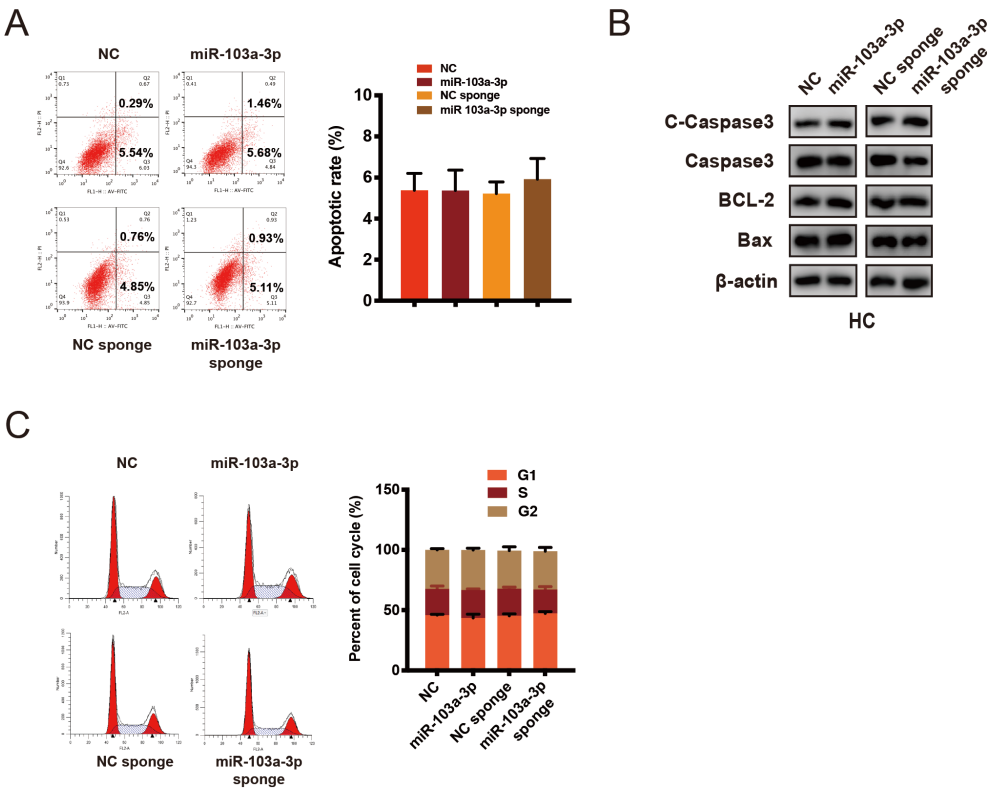

Supplementary Figure 7. miR-103a-3p is not related to apoptosis or the cell cycle. (A) HCs were transfected with miR-103a-3p, miR-103a-3p sponge or its negative control, stained with Annexin V-FITC and PI, and then subjected to flow cytometry detection. Representative images and histograms are shown. (B) The expression of apoptosis-associated proteins (cleaved-Caspase 3, Caspase 3, BCL-2 and Bax) was evaluated by Western blotting. (C) The proportions of cells at different cell cycle phases were evaluated by flow cytometry. The data were obtained from three independent experiments with three independent donors (presented as the means ± SDs) (A and C) or were representative of three independent experiments with similar results (B). (*P<0.05 and **P<0.01 vs the control or indicated group). The data were analyzed by two-tailed t-tests (A and C).

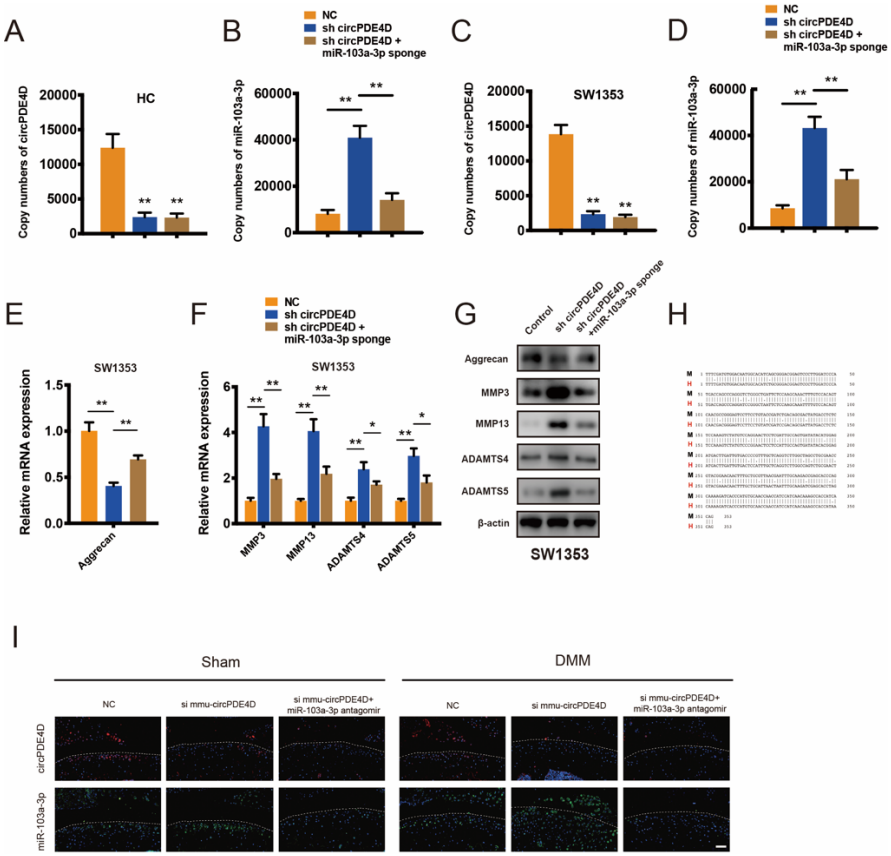

Supplementary Figure 8. miR-103a-3p reverses sh-circPDE4D-induced matrix degradation.

(A-B) HCs were stably transfected with empty vector (NC) or sh-circPDE4D or cotransfected with both sh-circPDE4D and miR-103a-3p sponge. The expression of circPDE4D and miR-103a-3p in HCs was evaluated by qRT-PCR. β-actin was used as an internal reference for mRNA, and U6 was used as an internal reference for miRNA. (C-D) SW1353 cells were stably transfected with empty vector (NC) or sh-circPDE4D or cotransfected with both sh-circPDE4D and miR-103a-3p sponge. The mRNA levels of circPDE4D and miR-103a-3p are shown in the histograms. (E-F) The mRNA expression of Aggrecan, MMP3, MMP13, ADAMTS4, and ADAMTS5 was evaluated by qRT-PCR. (G) The protein expression of Aggrecan and MMP3, MMP13, ADAMTS4, and ADAMTS5 was determined by Western blotting. (H) Sequence alignment of human circPDE4D (H) and the mouse circPDE4D homolog (M). (I) The expression of circPDE4D and miR-103a-3p in mouse cartilage was detected by FISH. miR-103a-3p probes were labeled with Alexa Fluor 488. Mmu-circPDE4D probes were labeled with CY3. Nuclei were stained with DAPI. Scale bar: 50 μm. The data were obtained from three independent experiments (presented as the means ± SDs) (A-F) or were representative of three independent experiments with similar results (G and I). (*P<0.05 and **P<0.01 vs the control or indicated group) The data were analyzed by two-tailed t-tests (A-F).

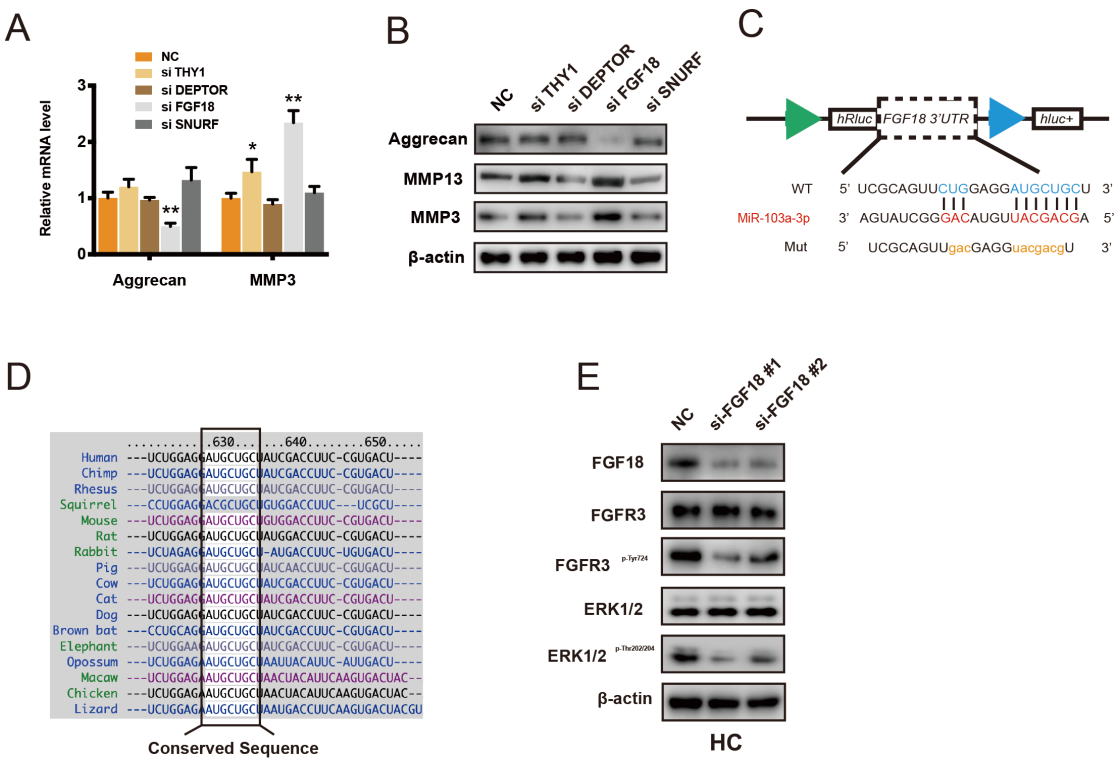

Supplementary Figure 9. FGF18 functions downstream of miR-103a-3p and plays a protective role in OA development.

(A) HCs were transfected with si-THY1, si-DEPTOR, si-FGF18, si-SNURF or negative control, and the changes in Aggrecan and MMP3 expression were evaluated by qRT-PCR. (B) Protein expression of Aggrecan, MMP3 and MMP13 after the knockdown of THY, DEPTOR, FGF18 or SNURF. (C) Schematic illustration demonstrating the complementary miR-103a-3p seed sequence with the FGF18 3'UTR. Lowercase letters indicate mutated nucleotides. (D) Sequence alignment of a putative miR-103a-3p-binding site within the 3'UTR of FGF18 mRNA revealed a high level of sequence conservation and complementarity with miR-103a-3p across vertebrates. (E) The protein expression of FGF18 and its downstream genes, including FGFR3, FGFR3$^{p\text{-}Tyr724}$, ERK1/2, and ERK1/2$^{p\text{-}Thr202/204}$, was determined by Western blotting. The data were obtained from three independent experiments with three independent donors (presented as the means ± SDs) (A) or were representative of three independent experiments with similar results (B and E). (*P<0.05 and **P<0.01 vs the control or indicated group) The data were analyzed by two-tailed t-tests (A).

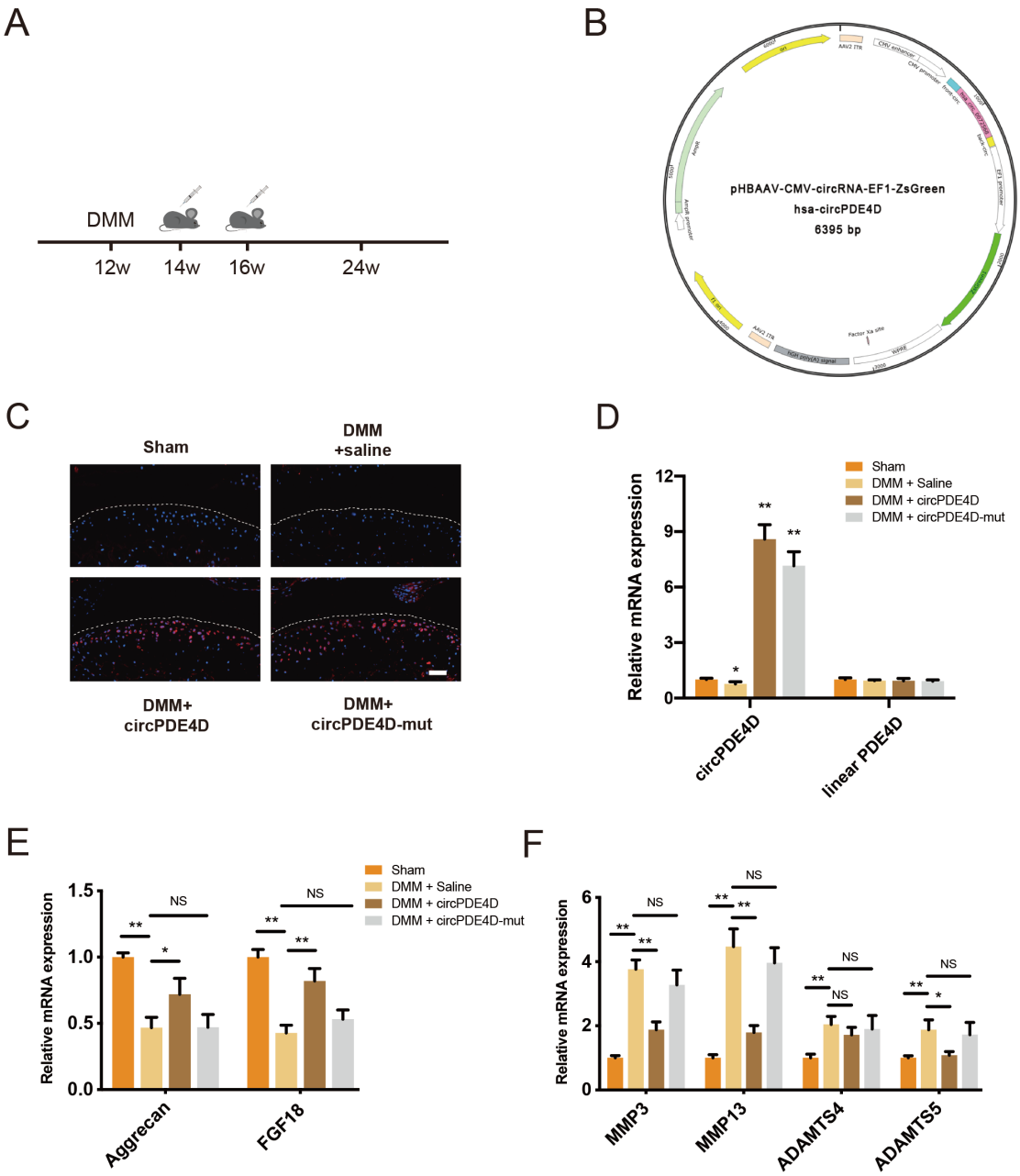

Supplementary Figure 10. Role of circPDE4D in the mouse DMM model.
(A) Schematic diagram demonstrating the timeline of the animal experiments. (B) Detailed information on the AAV. (C) The expression of circPDE4D (red) in mouse articular cartilage was detected. Representative images of FISH are shown. Scale bar: 50 μm. (D) The mRNA expression of circPDE4D and linear PDE4D in mouse cartilage was detected by qRT-PCR. (E-F) The expression of FGF18, catabolic enzymes (MMP3, MMP13, ADAMTS4 and ADAMTS5), and GAG composition (Aggrecan) in mouse cartilage tissues was determined by qRT-PCR. The data were presented as the means ± SDs (D-F) or were representative of three independent experiments with similar results (C). (*P<0.05 and **P<0.01 vs the control or indicated group) The data were obtained by two-tailed t-tests (D-F).

Supplemental Table 1 The information of patients

6 clinical cartilage tissues at stage 0						
Gender	Age (year)	Height (cm)	Weight (kg)	BMI	KL stage	KSS score
Female	40	155	54	22.48	0	N/A
Male	42	173	69	23.05	0	N/A
Female	48	157	58	23.53	0	N/A
Female	35	161	65	25.08	0	N/A
Male	39	171	69	23.60	0	N/A
Male	48	174	72	23.78	0	N/A
10 clinical cartilage tissues at stage 1						
Gender	Age (year)	Height (cm)	Weight (kg)	BMI	KL stage	KSS score
Male	63	176	76	24.54	2.3	66
Male	68	179	82	25.59	1.9	65
Male	70	170	68	23.53	2.5	67
Female	59	162	67	25.53	2.1	57
Female	59	162	69	26.29	2.2	65
Male	73	175	72	23.51	2.3	61
Female	59	158	59	23.63	2.2	62
Female	62	165	72	26.45	2.4	57
Female	57	162	61	23.24	1.9	61
Female	60	164	67	24.91	2.1	60
12 clinical cartilage tissues at stage 2						
Gender	Age (year)	Height (cm)	Weight (kg)	BMI	KL stage	KSS score
Male	69	167	71	25.46	2.5	56
Male	72	175	76	24.82	2.1	60
Female	73	165	68	24.98	2.5	43
Female	65	158	69	27.64	2.7	59
Female	63	157	62	25.15	2.1	68
Male	66	179	81	25.28	2.9	61
Female	71	155	66	27.47	2.3	63
Male	58	174	69	22.79	2.7	51
Female	59	161	73	28.16	2.6	53
Male	66	172	72	24.34	2.5	50
Female	64	156	63	25.89	2.3	54
Female	67	159	68	26.90	2.6	60
14 clinical cartilage tissues at stage 3						
Gender	Age (year)	Height (cm)	Weight (kg)	BMI	KL stage	KSS score
Male	59	176	70	22.60	2.7	48
Male	62	172	72	24.34	2.6	59
Male	69	181	80	24.42	2.7	59
Female	64	159	62	24.52	2.9	52
Female	70	166	67	24.31	2.9	44

Male	57	172	72	24.34	3.1	45
Female	54	162	71	27.05	3.1	49
Male	66	175	79	25.80	2.4	53
Female	55	164	62	23.05	2.7	45
Male	61	168	69	24.45	2.4	48
Female	67	164	59	21.94	2.5	49
Male	58	168	67	23.74	2.7	45
Female	69	161	64	24.69	2.6	60
Female	58	155	57	23.73	2.6	51
11 clinical cartilage tissues at stage 4						
Gender	Age (year)	Height (cm)	Weight (kg)	BMI	KL stage	KSS score
Female	66	155	59	24.56	3.2	41
Male	69	167	67	24.02	2.9	37
Male	71	169	66	23.11	3.1	45
Female	67	158	63	25.24	2.6	38
Male	69	176	69	22.28	2.8	37
Male	62	174	75	24.77	3.2	49
Female	61	160	65	25.39	2.9	49
Male	55	177	71	22.66	2.7	52
Female	67	154	62	26.14	2.9	37
Female	62	164	69	25.65	2.5	42
Male	57	173	74	24.73	3.1	48
Other cartilage tissues used for primary chondrocytes culture						
Gender	Age (year)	Height (cm)	Weight (kg)	BMI	KL stage	KSS score
Male	57	175	75	24.49	2.1	63
Male	62	174	73	24.11	2.4	58
Male	67	172	73	24.68	2.6	58
Female	64	162	62	23.62	2.7	54
Female	59	158	62	24.84	2.2	62
Male	62	174	69	22.79	2.8	49
Female	66	168	63	22.32	2.7	54
Male	65	165	60	22.04	2.5	55
Female	61	156	58	23.83	2.3	59